NASA/TM–2005-213458

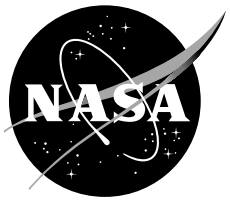

Effects of Swept Tips on V-22 Whirl Flutter and Loads

C. W. Acree, Jr.
Ames Research Center, Moffett Field, California

May 2005

The NASA STI Program Office . . . in Profile

Since its founding, NASA has been dedicated to the advancement of aeronautics and space science. The NASA Scientific and Technical Information (STI) Program Office plays a key part in helping NASA maintain this important role.

The NASA STI Program Office is operated by Langley Research Center, the Lead Center for NASA's scientific and technical information. The NASA STI Program Office provides access to the NASA STI Database, the largest collection of aeronautical and space science STI in the world. The Program Office is also NASA's institutional mechanism for disseminating the results of its research and development activities. These results are published by NASA in the NASA STI Report Series, which includes the following report types:

- TECHNICAL PUBLICATION. Reports of completed research or a major significant phase of research that present the results of NASA programs and include extensive data or theoretical analysis. Includes compilations of significant scientific and technical data and information deemed to be of continuing reference value. NASA's counterpart of peer-reviewed formal professional papers but has less stringent limitations on manuscript length and extent of graphic presentations.

- TECHNICAL MEMORANDUM. Scientific and technical findings that are preliminary or of specialized interest, e.g., quick release reports, working papers, and bibliographies that contain minimal annotation. Does not contain extensive analysis.

- CONTRACTOR REPORT. Scientific and technical findings by NASA-sponsored contractors and grantees.

- CONFERENCE PUBLICATION. Collected papers from scientific and technical conferences, symposia, seminars, or other meetings sponsored or cosponsored by NASA.

- SPECIAL PUBLICATION. Scientific, technical, or historical information from NASA programs, projects, and missions, often concerned with subjects having substantial public interest.

- TECHNICAL TRANSLATION. English-language translations of foreign scientific and technical material pertinent to NASA's mission.

Specialized services that complement the STI Program Office's diverse offerings include creating custom thesauri, building customized databases, organizing and publishing research results . . . even providing videos.

For more information about the NASA STI Program Office, see the following:

- Access the NASA STI Program Home Page at *http://www.sti.nasa.gov*

- E-mail your question via the Internet to help@sti.nasa.gov

- Fax your question to the NASA Access Help Desk at (301) 621-0134

- Telephone the NASA Access Help Desk at (301) 621-0390

- Write to:
  NASA Access Help Desk
  NASA Center for AeroSpace Information
  7121 Standard Drive
  Hanover, MD 21076-1320

NASA/TM–2005-213458

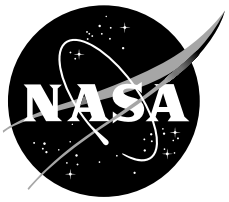

Effects of Swept Tips on V-22 Whirl Flutter and Loads

C. W. Acree, Jr.
Ames Research Center, Moffett Field, California

National Aeronautics and
Space Administration

Ames Research Center
Moffett Field, California 94035-1000

May 2005

Acknowledgments

The author wishes to thank Wayne Johnson for his unfailing support and encouragement for this research, and David A. Popelka for his generous assistance in providing data and advice for modeling the V-22.

Available from:

NASA Center for AeroSpace Information
7121 Standard Drive
Hanover, MD 21076-1320
(301) 621-0390

National Technical Information Service
5285 Port Royal Road
Springfield, VA 22161
(703) 487-4650

Table of Contents

NOMENCLATURE

Symbols:

C_{l_α}	lift-curve slope
C_P	rotor power coefficient
C_T	rotor thrust coefficient
M_{tip}	tip Mach number
r	radial station
r_s	radial station at start of sweep
R	rotor radius
x_m	tip-mass offset, positive forward
Λ	sweep angle, positive aft
δ_3	kinematic pitch-flap coupling angle

Abbreviations:

ASAP	Aeroelastic Stability Analysis of Proprotors
CAMRAD	Comprehensive Analytical Model of Rotorcraft Aerodynamics and Dynamics
CFD	computational fluid dynamics
EMD	Engineering and Manufacturing Development
hpp	half peak-to-peak
KTAS	knots true airspeed
NASTRAN	NASA Structural Analysis
SHP	shaft horsepower

Wing/Fuselage Modes:

ABT	afterbody torsion
APY	antisymmetric pylon yaw
AWB	antisymmetric wing beamwise bending
AWC	antisymmetric wing chordwise bending
AWT	antisymmetric wing torsion
SPY	symmetric pylon yaw
SWB	symmetric wing beamwise bending
SWC	symmetric wing chordwise bending
SWT	symmetric wing torsion

EFFECTS OF SWEPT TIPS ON V-22 WHIRL FLUTTER AND LOADS

C. W. Acree, Jr.

Ames Research Center

SUMMARY

A CAMRAD II model of the V-22 Osprey tiltrotor was constructed for the purpose of analyzing the effects of blade design changes on whirl flutter. The model incorporated a dual load-path grip/yoke assembly, a swashplate coupled to the transmission case, and a drive train. A multiple-trailer free wake was used for loads calculations. The effects of rotor design changes on whirl-mode stability were calculated for swept blades and offset tip masses. A rotor with swept tips and inboard tuning masses was examined in detail to reveal the mechanisms by which these design changes affect stability and loads. Certain combinations of design features greatly increased whirl-mode stability, with (at worst) moderate increases to loads.

INTRODUCTION

Tiltrotor designs are constrained by aeroelastic stability requirements, specifically by the need to avoid whirl flutter. With current technology, this requires very stiff, thick wings of limited aspect ratio, limiting cruise efficiency and maximum speed. The rotor design is also constrained in such areas as control-system kinematics. Numerous approaches to improving the whirl-mode airspeed boundary have been investigated, including active stability augmentation (ref. 1) and aeroelastic tailoring of wings and rotors (refs. 2–4). The research reported here applies the purely passive approaches of sweeping the outboard blade sections and moving tip balance weights forward.

Improving proprotor whirl-mode stability margins is an ongoing research activity at NASA Ames Research Center. Previous publications presented results for the XV-15 (ref. 5), and initial results for the V-22 (refs. 6 and 7). The present paper includes results for an updated V-22 CAMRAD II model (Comprehensive Analytical Model of Rotorcraft Aerodynamics and Dynamics, ref. 8) with a multiple-trailer free wake (ref. 9) and other improvements, applied to rotors with swept tips and chordwise tip-mass offsets. It is an expanded version of reference 10, with additional figures and an appendix documenting the wake model. Material from reference 11 is also included, in order to provide a more complete description of the CAMRAD II model. Example jobs are given in the appendix.

This paper begins with a discussion of the V-22 CAMRAD II model, followed by whirl-flutter predictions for the baseline V-22 rotor. Then follow discussions of rotor design modifications, including δ_3 variations (to deliberately destabilize the baseline rotor) and idealized models of swept blades and tip-mass offsets. The most practical combination of design changes—swept tips with an inboard tuning mass—is examined in some detail for stability, and briefly for loads. This paper also examines the mechanisms by which sweep and tip-mass offsets affect whirl flutter. The paper concludes with suggestions for further research and associated model improvements.

V-22 CAMRAD II MODEL

The V-22 rotor is stiff in-plane with a gimbaled hub and –15 deg pitch-flap coupling (δ_3). The structure is mostly composite, with a coning flexure and blade-fold hinges. The aerodynamic sections start with a 36-in. chord at 5% radius, linearly tapering to a 22-in. chord at the tip. The taper is interrupted by a bump over the blade-fold hinge. Total effective blade twist is 47.5 deg over a 228.5-in. radius. The quarter-chord locus is swept about 1 deg aft, with the quarter-chord line intersecting the pitch axis at 75% radius.

The V-22 tiltrotor was modeled with CAMRAD II Release 4.1 (ref. 8). The rotor model is shown in Figure 1. Rotor airfoil shapes are shown in figure 1 merely to better reveal the blade twist, and do not capture the details of the inboard fairings; CAMRAD II derives its aerodynamic data from airfoil tables (C81 format).

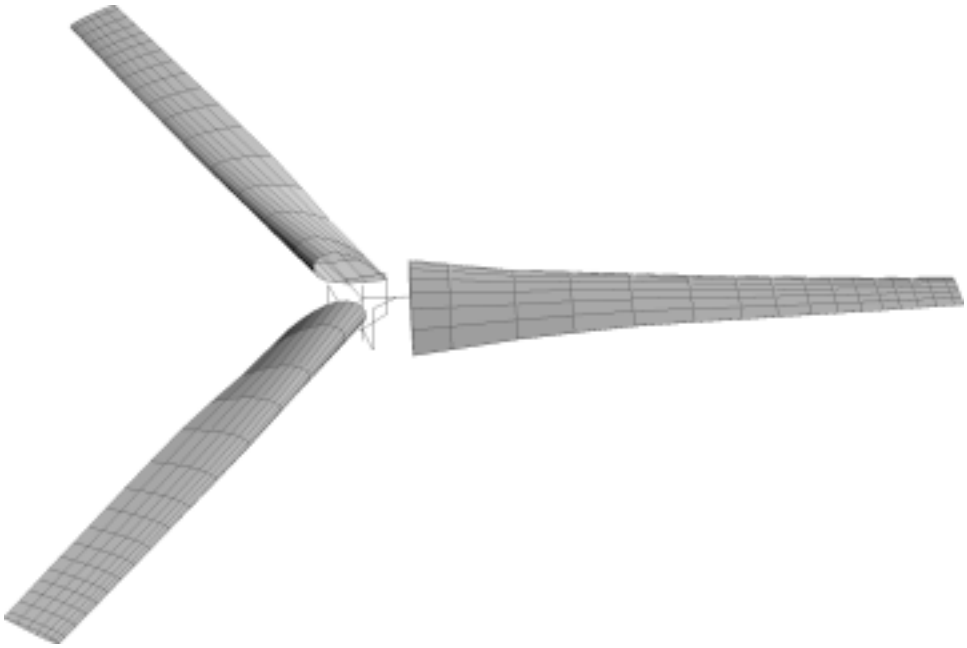

Figure 1. CAMRAD II model of the V-22 rotor.

Considerable effort went into modeling the V-22 yoke and grip (fig. 2). The V-22 hub comprises three composite arms, or yokes, connected to the shaft by a constant-velocity joint. The yokes gimbal as a unit, but do not pitch with the blades. Centrifugal loads and flap and lag moments are carried by the yokes. Pitching moments, hence control loads, for each blade are carried by a hollow pitch case (“grip”) that surrounds the yoke and pitches with the blade. The blades are attached to the outer ends of the grips.

Each yoke is much less stiff in flap than in lag, such that it constitutes a coning flexure; the zero-load precone is 2.75 deg. The large lag stiffness places the first lag frequency above 1/rev for all flight conditions, so that the rotor is by definition stiff in-plane.

The grip is connected to the yoke by a series of elastomeric bearings that accommodate the large changes in pitch needed between hover and high-speed flight. Two pitch-change bearings at (approximately) the inboard and outboard ends of the yoke accommodate blade pitch and transmit shear loads from the grip to the yoke. A separate bearing restrains the blade against centrifugal loading. The elastomeric bearings allow a small

amount of in-plane and out-of-plane cocking of the grip with respect to the yoke, in order to accommodate flexing of the yoke as the coning angle changes.

The V-22 CAMRAD II model is based on four sets of data:

1. Rotor structural data provided by Bell Helicopter Textron (ref. 12), originally developed for Bell Helicopter's Myklestad program.

2. Rotor aerodynamic data, in the form of C81 tables, also provided by Bell Helicopter. The C81 tables are based on wind-tunnel test data of the rotor airfoils (ref. 13).

3. Airframe geometry, converted from an earlier model developed by Boeing Helicopters for the CAMRAD/JA version of CAMRAD.

4. Airframe modal data for the V-22, provided by Bell Helicopter (ref. 12; see also ref. 14). The data were generated by "SuperElement" models using the NASA Structural Analysis program, as developed by the MacNeal-Schwendler Corporation (MSC/NASTRAN).

Additional data (unpublished) were provided by David A. Popelka and Jim C. Narramore of Bell Helicopter. The rotor modeled is the Engineering and Manufacturing Development (EMD) version.

Further details of the model are discussed in the following paragraphs, which apply to whirl-flutter calculations. Loads analyses use a free-wake model and other features, which are discussed in the Loads section of this paper.

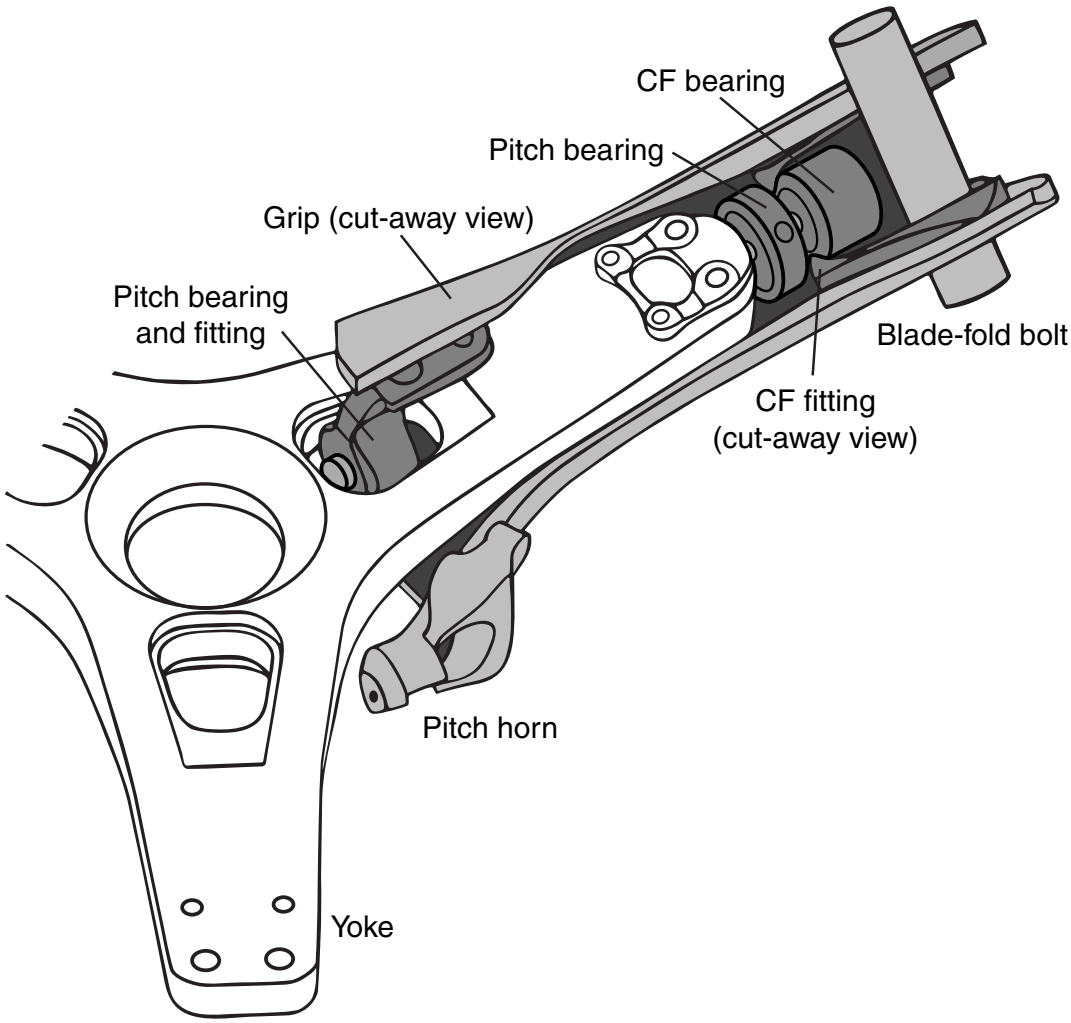

Figure 2. V-22 rotor yoke and grip; pitching components are shaded.

Rotor Model

The CAMRAD II model of the V-22 is documented in detail in reference 11. A summary of key features follows.

The CAMRAD II model of the V-22 is an evolution of that in reference 6. For the analyses reported herein, several improvements to the model were made, including a refined dual load-path hub and a more sophisticated control-system stiffness model. Also, the blade frequencies were matched to adjusted test data, instead of to Myklestad predictions.

The blade-frequency data are for a nonrotating test of the entire V-22 rotor, with all three blades but without the gimbal, drive train, or control system (ref. 15). Therefore, the root boundary conditions are considerably different from those for the complete aircraft. Moreover, the test did not use production blades. To allow a comparison of the CAMRAD II predictions, error ratios between the Myklestad nonrotating predictions and the test data were calculated, and then the Myklestad rotating predictions were corrected by the same ratios to generate new target frequencies. For example, the lag mode at 6.79 Hz (Myklestad prediction) was increased by 2.00% to get a target frequency of 6.93 Hz.

Release 4.1 of CAMRAD II provides multiple options for dual-load-path models. The option most appropriate for modeling the V-22 grip/yoke assembly specifies the flexbeam/blade connection (via the snubber) in flexbeam-oriented axes. Using this model, the blade frequencies were matched to Myklestad predictions, adjusted for test data. The new V-22 model also had corrected zero-torque angles for the elastomeric pitch bearings.

The hub/yoke model has a rigid hub extending to the inboard pitch bearing, and two elastic beam elements, representing the yoke, between the bearings. The blade model has four elastic beam elements, starting at the inboard pitch bearing: the grip is modeled as a single element, and the rest of the blade with three elements. The outermost blade element spans the swept section.

The blade model has 17 aerodynamic panels, each with collocation points at 1/4 and 3/4 chord (used by first- and second-order lifting line theory, respectively). This is more panels than would normally be used for whirl-flutter calculations, but a finer distribution is appropriate to capture the effects of blade sweep. Uniform inflow is adequate for whirl-flutter analyses and was used for all stability calculations.

Control-System Stiffness

The previous model (ref. 6) used a single value of net control-system flexibility, input as pitch-link stiffness. The new model has separate rotating and nonrotating stiffnesses (pitch link and swashplate, respectively). Furthermore, the fixed-system stiffness has distinct collective and cyclic values.

The Myklestad program uses table lookups to determine separate collective and cyclic control-system stiffnesses at each blade pitch angle (collective trim angle). The stiffness tables were derived from test data of the actual control system. Myklestad computes the collective and cyclic frequencies separately, with different control-system stiffness values as defined by the lookup table (ref. 12).

In contrast, CAMRAD II provides for separate collective and cyclic nonrotating stiffnesses, referenced to the swashplate, plus a rotating pitch-link stiffness. The complete kinematics of the swashplate, pitch link, and

pitch horn are modeled. However, the model did not include minor, local nonlinearities in the swashplate and actuator stiffnesses that arise as the actuators extend and retract. CAMRAD II computes the collective and cyclic frequencies together, using the total effective pitch stiffness as determined by the control-system kinematics. Hence, CAMRAD II cannot perfectly match the Myklestad control-system stiffness values, but can model the nonlinear kinematics. The swashplate actuators are coupled to the transmission case, so that the swashplate motion is determined by the airframe mode shapes at the transmission, not the hub (ref. 6).

Figure 3 schematically illustrates the CAMRAD II control-system stiffness model. The swashplate is modeled as rigid, but can translate along the rotor shaft for collective inputs, and pivot for cyclic inputs. There is a cyclic spring, plus a linear spring for collective. CAMRAD II can have separate lateral and longitudinal cyclic spring rates, but these were made equal in the present V-22 model.

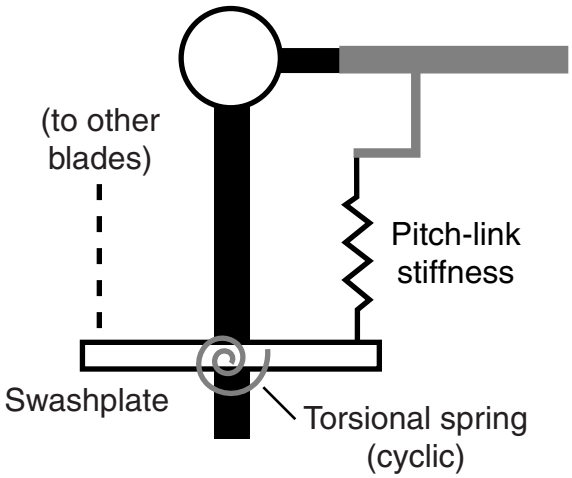

Figure 3. Control-system model with separate rotating- and fixed-system stiffnesses.

Airframe Model

To calculate aeroelastic stability, CAMRAD II couples externally generated wing/pylon modes to an internally generated dynamic rotor model (ref. 8). The wing/pylon modes were generated by a three-dimensional NASTRAN shell model (about 68,000 elements), with frequency adjustments based on flight- and ground-test data (ref. 12). The structural damping of each mode was adjusted in accordance with test data, then increased by a constant value to approximate the effects of wing aerodynamic damping as given in reference 12.

The drive-train model included the engine and gearbox rotational inertias, drive-shaft and cross-shaft flexibilities, but no governor (the governor was not needed for trim or whirl flutter analyses).

Trim and Flutter Models

Except where noted, the model was trimmed to zero power (windmill state). Zero power is typically the least stable flight condition for tiltrotors, and the drive train affects certain boundary conditions for blade modes. The V-22 has a flapping controller that minimizes flapping in flight; this was modeled in CAMRAD II

simply by assuming axisymmetric, axial flow and by trimming to zero power with collective. This automatically yielded zero flapping. A further simplification was to trim the rotor to zero power in level flight and the airframe to zero angle of attack, essentially ignoring airframe aerodynamics. Given the assumptions of axisymmetric flow and zero power, there was little to be gained by explicitly trimming the airframe. The automatic flight control system was not needed for trim and was not modeled. The rotor was trimmed to 332 rpm at 7500-ft (2300-m) altitude to match the Aeroelastic Stability Analysis of Proprotors (ASAP) predictions in reference 12.

For trim, blade deflections are calculated using nine flexible degrees of freedom per element (the CAMRAD II default).

Flutter calculations included a gimbal for each rotor, nine airframe modes, and seven drive-train modes (representing all drive-train components except the governor). The blade flutter model used 12 dynamic modes per blade (the 12 lowest frequencies, up to 174 Hz, or 31/rev uncoupled). The airframe modes included wing beamwise and chordwise bending, wing torsion, and pylon yaw, separated into symmetric and antisymmetric modes, and the afterbody torsion mode; the airframe frequencies ranged from 2.9 to 8.6 Hz. The drive-train model included separate rotor-, engine- and cross-shaft torsional flexibilities plus rotor, engine, shaft, and gearbox rotational inertias.

Baseline Predictions

Figures 4–7 show the whirl-flutter predictions for the baseline CAMRAD II model. Frequency and damping are plotted against airspeed for symmetric and antisymmetric modes. These predictions are for level flight at zero power. Tracking the modes is problematic at high speeds because of the strong modal couplings, including multiple frequency crossings. Fortunately, the ambiguities are limited to high-frequency modes that do not determine the flutter boundary; therefore, no significant effort was made to track and label all modal couplings. Furthermore, damping predictions above 400 knots are of limited accuracy because of limitations of the airfoil tables (refs. 6 and 11).

Trends are plotted in figures 4–7 for wing beamwise, chordwise, and torsion modes, and for pylon yaw modes, all in symmetric and antisymmetric forms. The afterbody torsion mode and rotor gimbal modes are also shown. The gimbal modes are shown in figures 4 and 5 to indicate their effects on the symmetric wing beamwise bending (SWB) and antisymmetric chord bending (AWC) modes. The gimbal modes are highly damped and well off the scales of figures 6 and 7. The peak in the AWC mode (fig. 7) is caused by an interaction with the gimbal mode.

All modes are stable at all airspeeds, and with one exception have favorable trends. The exception is SWB (fig. 6), which is just barely stable at about 360 knots. The dramatic increase above this speed is caused by compressibility effects. If this minimum stability margin could be increased, it would relax important constraints on the rotor design. (The V-22 rotor had to be redesigned as a result of inadequate stability margins, as measured during a wind-tunnel test (ref. 16).) This is the primary motivation for the present research.

The SWB mode has the smallest stability margin within the V-22 flight envelope, so it is the appropriate mode against which to test the effects of model variations, as discussed in the following sections. Because zero-power trim has the lowest damping for critical modes within the flight envelope, it is appropriate for this study and was used for all predictions reported herein.

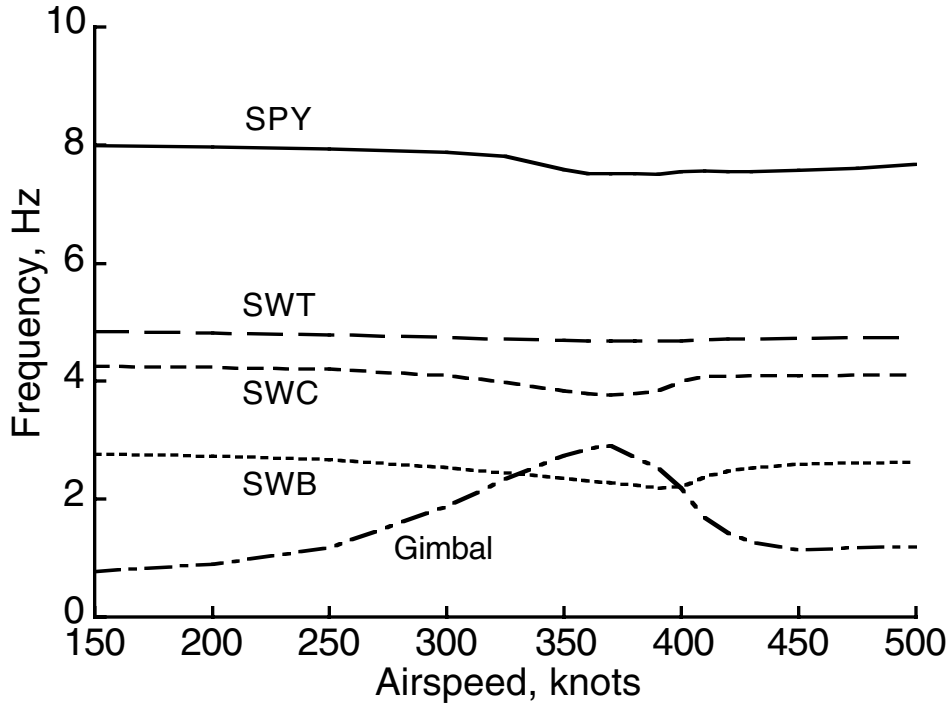

Figure 4. Predicted frequencies of the V-22 symmetric wing/pylon modes.

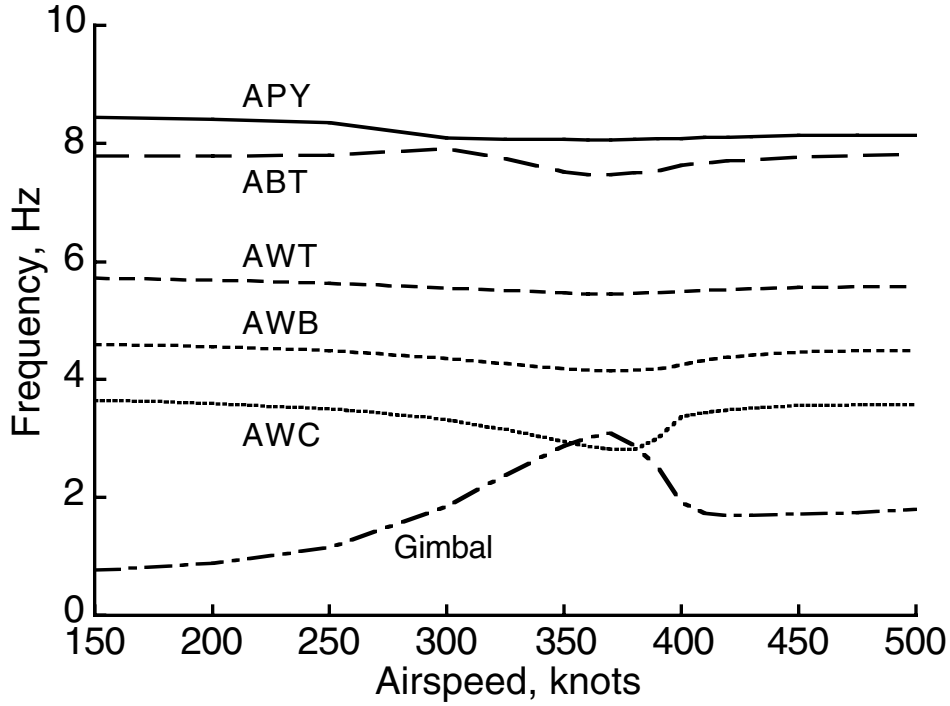

Figure 5. Predicted frequencies of the V-22 antisymmetric wing/pylon modes.

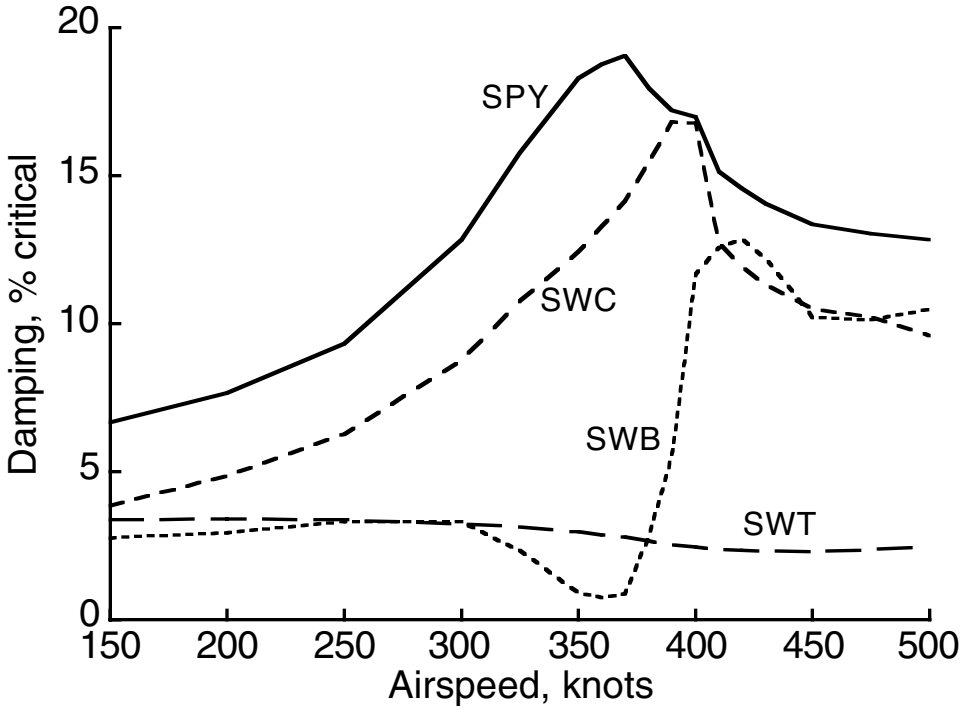

Figure 6. Predicted damping of the V-22 symmetric wing/pylon modes.

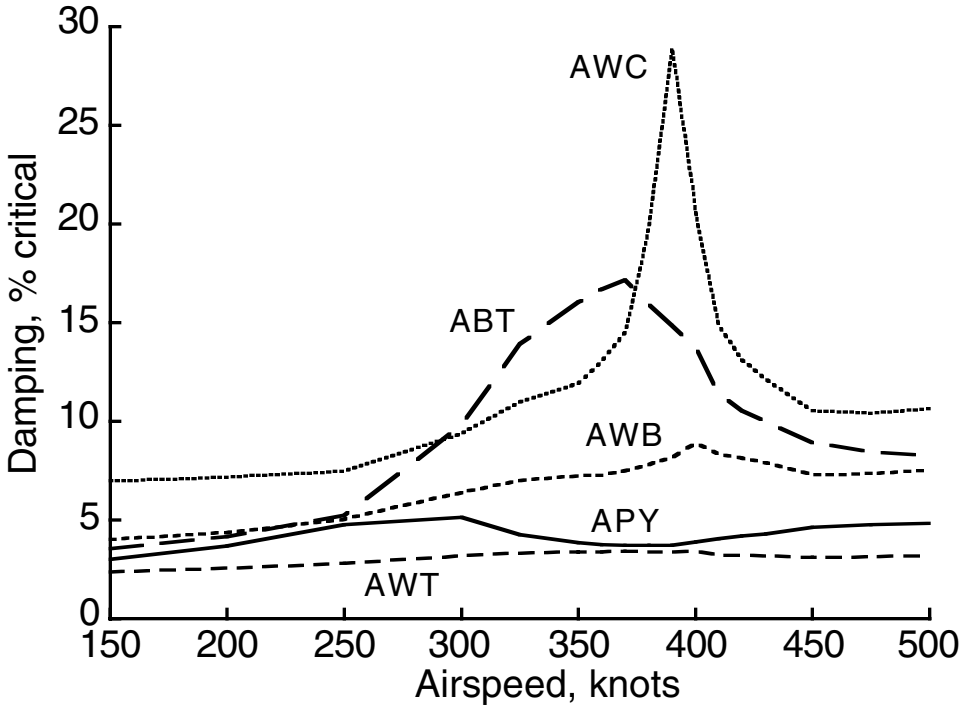

Figure 7. Predicted damping of the V-22 antisymmetric wing/pylon modes.

Reference 6 reports the application of an earlier model to blade design changes for improving whirl-flutter margins. Subsequent to that publication, an error was discovered in the CAMRAD II analysis code that affected stability calculations for dual-load-path hubs at very large collective angles (a flight condition unique to tiltrotors). All predictions reported herein were recalculated with corrected code, hence they do not generally match those of reference 6. The new calculations were used as an opportunity to further improve the model, as discussed previously in the Rotor Model and Control-System Stiffness sections.

EFFECTS OF DESIGN VARIATIONS

This section examines the mechanisms by which sweep affects whirl flutter. Broadly speaking, blade design changes can affect stability either by altering the forces and moments on the blade or by altering the dynamic response to those forces and moments. Detail mechanisms include (1) alteration of inertial coupling about the pitch axis, (2) reduction of local lift-curve slope, (3) effective mass droop at high pitch angles, (4) alteration of unsteady loads, and (5) alteration of blade mode shapes and frequencies. These are examined for a variety of idealized blade models, followed by a practical design. It will be shown that the first and last effects are the most important.

Whirl-mode stability is also affected by kinematic couplings between the blades, hub, and control system. Because the V-22 hub geometry is tightly constrained, improving stability by altering such couplings is unrealistic. Instead, altered kinematics were used to destabilize the baseline design, as explained in the following sections.

Delta-3 Effects

Because it is already stable, the baseline model (figs. 4–7) is not convenient for analyzing the effects of rotor design on aeroelastic stability. The effects of such design changes can be nonlinear, so it is more appropriate to use a baseline that is moderately unstable than to further increase stability of stable modes. Although analyzing whirl flutter with a more flexible, hence less stable wing would be physically realistic, it would require significant changes to the V-22 NASTRAN model in order to generate consistent mode shapes. However, it is a simple matter to destabilize the rotor by changing the pitch/flap coupling (δ_3). As defined herein, positive δ_3 causes nose-down pitching for upward blade flapping (fig. 8). The V-22 has negative δ_3, as shown in figure 8.

For the present study, δ_3 was always changed by adjusting the distance of the pitch horn from the flapping axis, so that the distance from the pitch axis remained constant. Such a modification does not affect the structure or aerodynamics of the individual blades, so its effects on aeroelastic stability are not confounded with those of the other design changes considered in the following discussion.

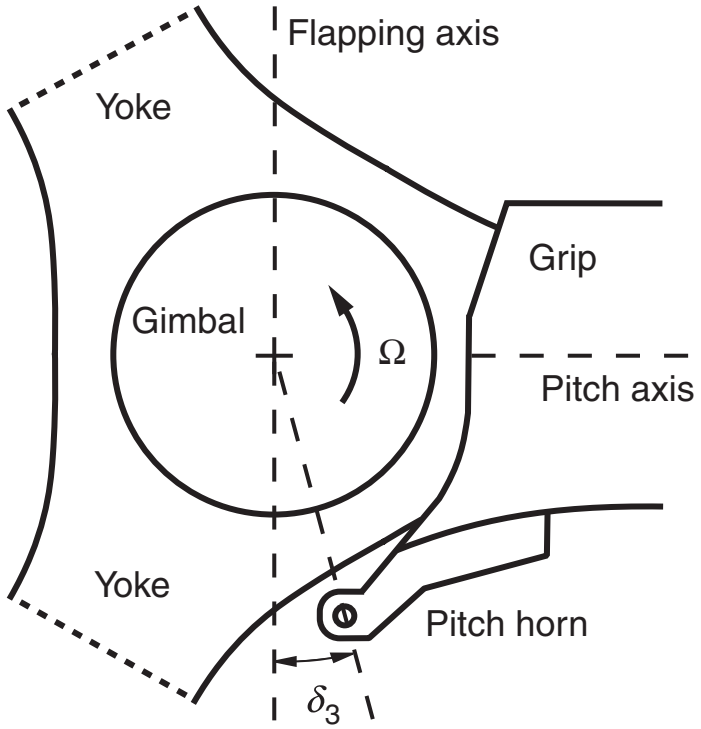

Figure 8. Kinematics of V-22 hub and pitch horn, showing design δ_3 of –15 deg.

Figures 9 and 10 show the effects on whirl modes of changing δ_3; only adversely affected modes are shown. The first lag mode rapidly becomes unstable for positive values of δ_3 (ref. 17), and larger negative values of δ_3 are desirable for new rotor designs, so only negative values of δ_3 were examined here. A reference airspeed of 300 knots was chosen to keep the rotor within its design envelope, but near the upper limit.

The trend in stability follows the classic pattern: the rotor remains stable until δ_3 approaches –20 deg, then the least stable mode (in this case, the SWB mode) rapidly loses stability as the magnitude of δ_3 becomes more negative. At large values of δ_3, the symmetric wing chord and pylon modes show similar trends toward instability as the SWB mode. The torsion modes vary only slightly and are not shown. AWC is the most sensitive mode, but at zero δ_3 it is more stable than SWB, so it is not the critical mode. AWB and ABT show similar trends at high δ_3. Two highly coupled modes, both involving primarily pylon yaw and gimbal whirl modes, have nearly identical values, with near-zero stability at –45 deg δ_3.

The δ_3 values shown here are for a level pitch horn; the actual value varies slightly with blade pitch. The design value of δ_3 for the V-22 is –15 deg, which provides an adequate stability margin. A value of –30 deg was chosen for the design studies discussed in the following paragraphs. The challenge is to stabilize the SWB and AWC modes without degrading the other modes.

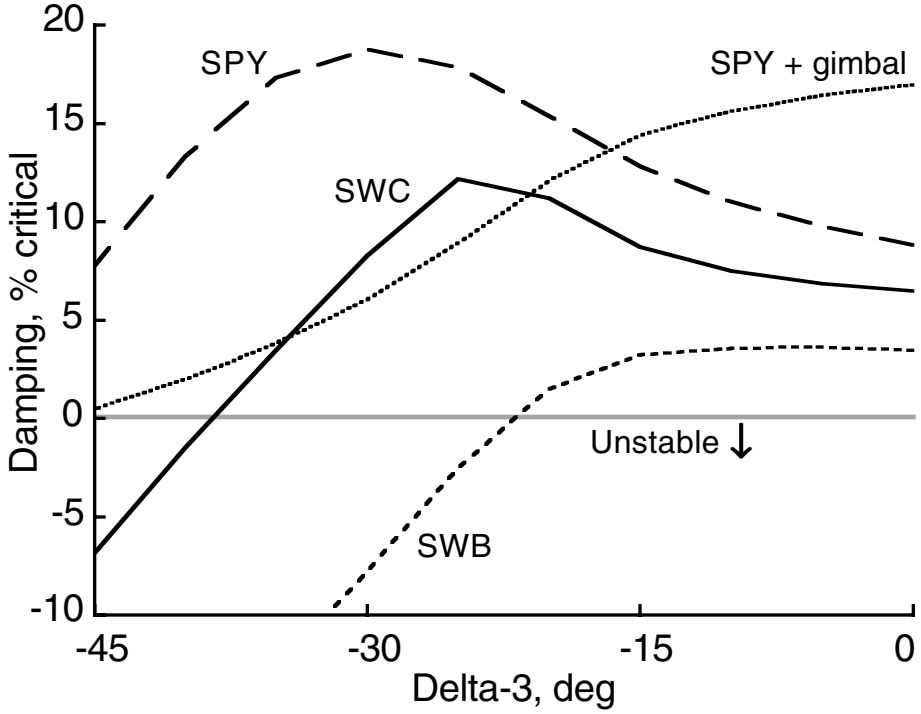

Figure 9. Variation of damping with δ_3 for the unmodified V-22 rotor at 300 knots. Only adversely affected symmetric modes are shown.

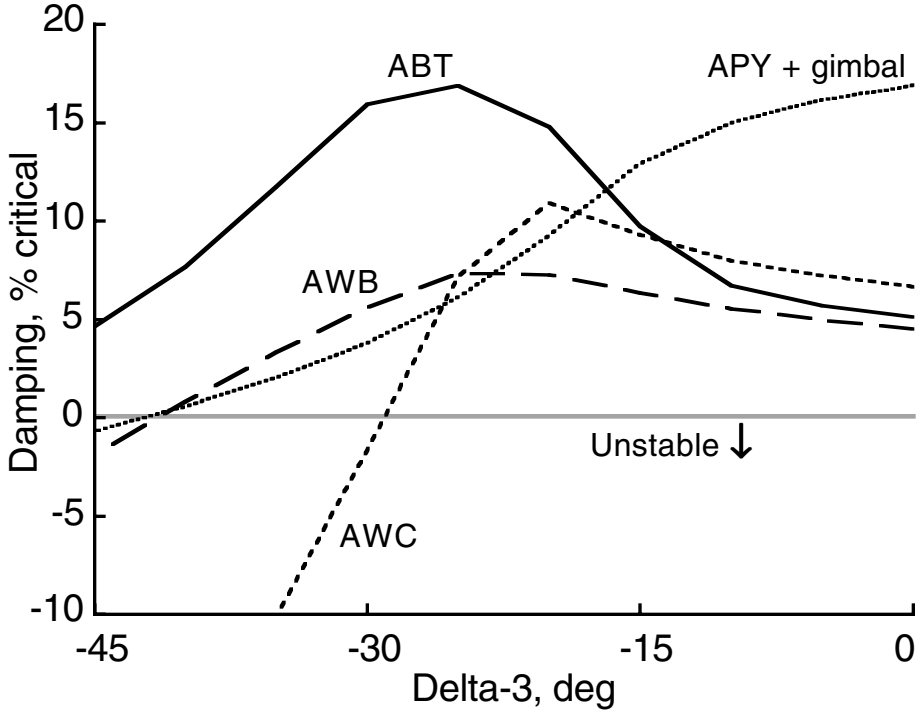

Figure 10. Variation of damping with δ_3 for the unmodified V-22 rotor at 300 knots. Only adversely affected antisymmetric modes are shown.

Blade Sweep

To stabilize the rotor with –30 deg δ_3, combinations of blade sweep and tip-mass offset were studied. Figure 11 shows several example blades derived from the V-22 rotor. For this rotor, the primary significance of sweep is the improved whirl-flutter boundary, not the reduced Mach-number effects. An offset tip mass is also shown; it is simply the existing balance weight moved forward from its normal position. The balance weight is normally located slightly inboard of the tip, as shown.

For this CAMRAD II model, blade sweep was invoked by sweeping the elastic axis and airfoil quarter-chord line by a sweep angle Λ, positive aft, starting at a radial station r_s. For these initial studies, r_s was always 80% R (rotor radius). The tip mass was offset from its design location a distance x_m, positive forward. The entire mass was always moved. Sweep was always calculated in the local chord plane, so it follows the blade twist. Tip-mass offsets were also always in the local chord plane. The maximum sweep shown here is equivalent to less than one chord length at the tip.

For convenient comparisons to blade sweep, tip-mass offset x_m is presented here in terms of equivalent sweep Λ, where

$$\Lambda = \sin^{-1}\left(\frac{x_m}{R - r_s}\right)$$

For pure blade sweep (fig. 11(b)), the tip mass was offset aft of the pitch axis with the rest of the blade so that it maintained the same position with respect to the elastic axis. For pure tip-mass offsets (fig. 11(c)), the tip mass was offset forward of the pitch axis.

Sweep was always calculated in the local chord plane, so it follows the blade twist. Tip-mass offsets were also always in the local chord plane. The maximum sweep analyzed here is equivalent to less than one chord length at the tip.

Figures 12 and 13 show the effects of sweep and tip-mass offsets on damping. The magnitudes of blade sweep and tip-mass equivalent sweep are the same, but the signs are reversed. Most modes were little affected and are not shown. The most responsive modes—SWB and AWC—were the least stable, which is encouraging. Note that the effects of sweep on damping are nonlinear, unlike the effects of tip-mass offset.

Figure 14 illustrates the effects of combining sweep and tip-mass offset, with the forward tip-mass offset of figure 13 added to the aft blade sweep of figure 12. Sweep and mass offset were incremented by the same magnitudes but opposite signs. The response of the SWB mode is slightly nonlinear. The SWT mode damping decreases very slightly with sweep, so that the optimum value of sweep is about 27 deg.

Figure 15 shows the effects of sweep with the tip mass fixed at its original position with respect to the blade pitch axis, which is perhaps a more practical configuration. The damping is much improved compared to that with sweep alone (fig. 12), although the SWB mode never becomes stable.

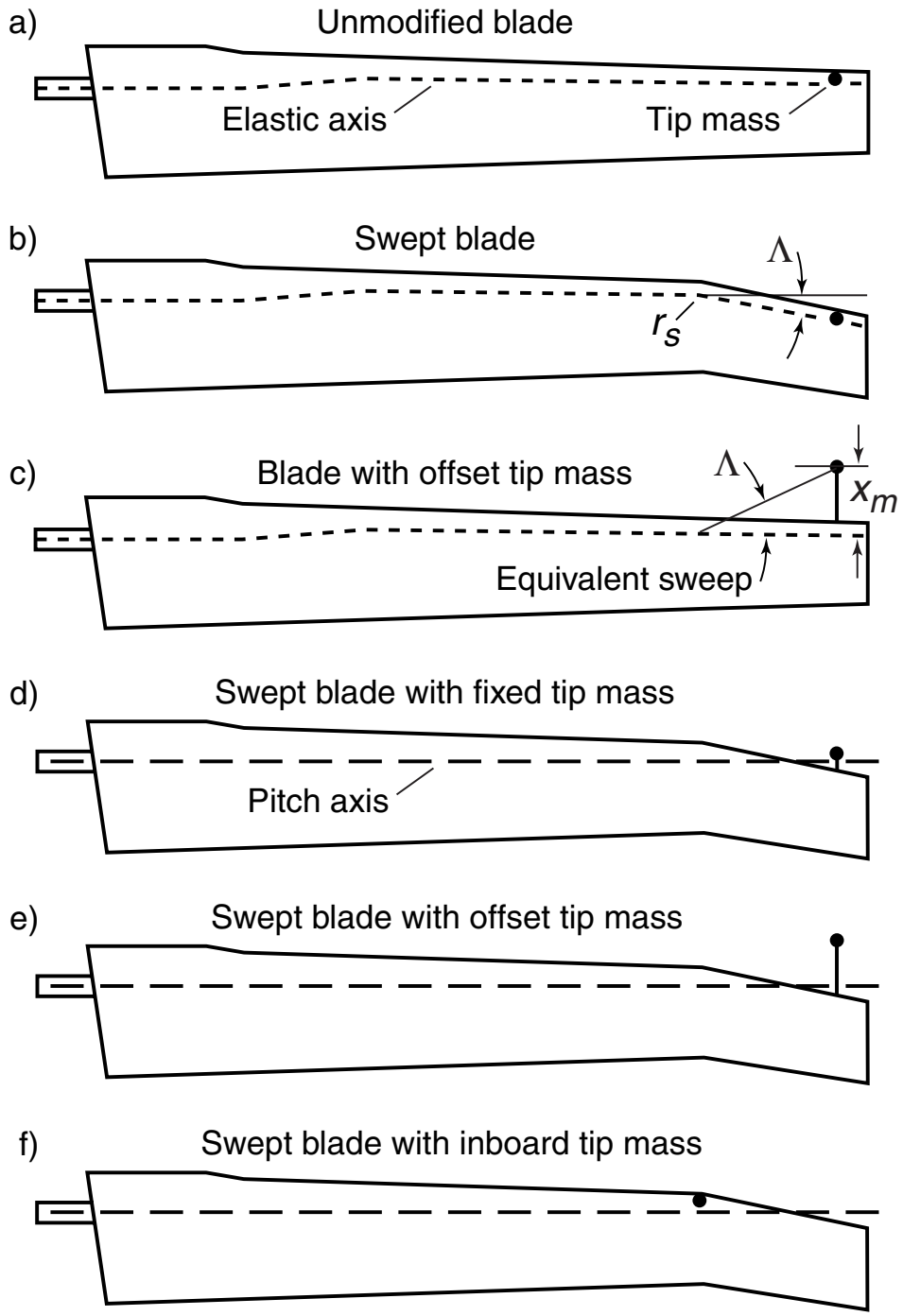

Figure 11. V-22 rotor blade planform (47.5-deg twist not shown).

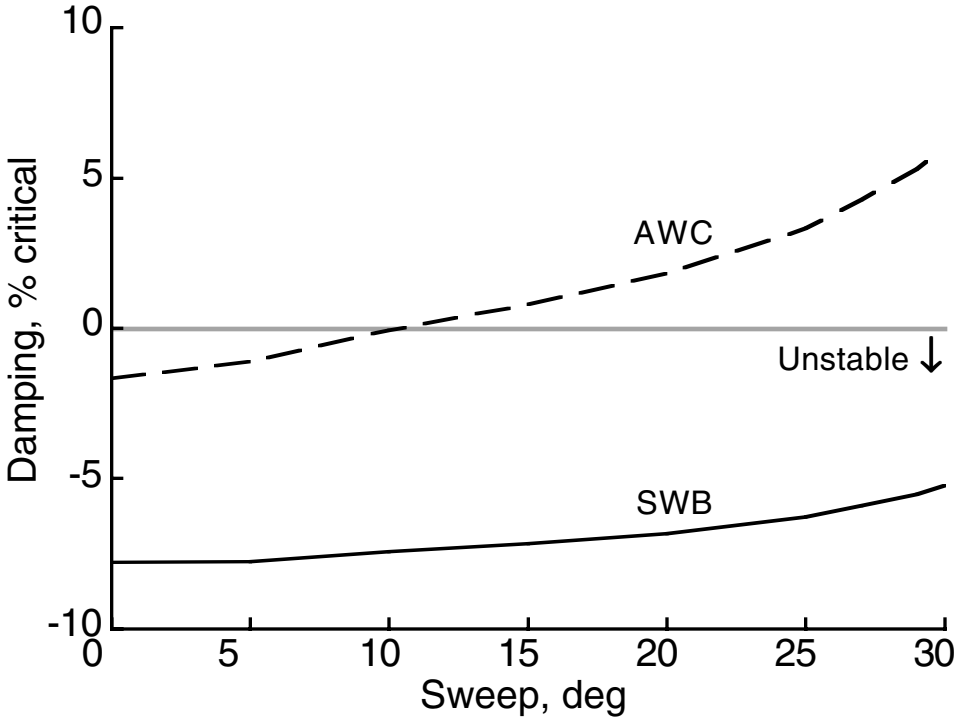

Figure 12. Variation of damping with blade sweep at 300 knots with –30 deg δ_3 (see fig. 11(b)).

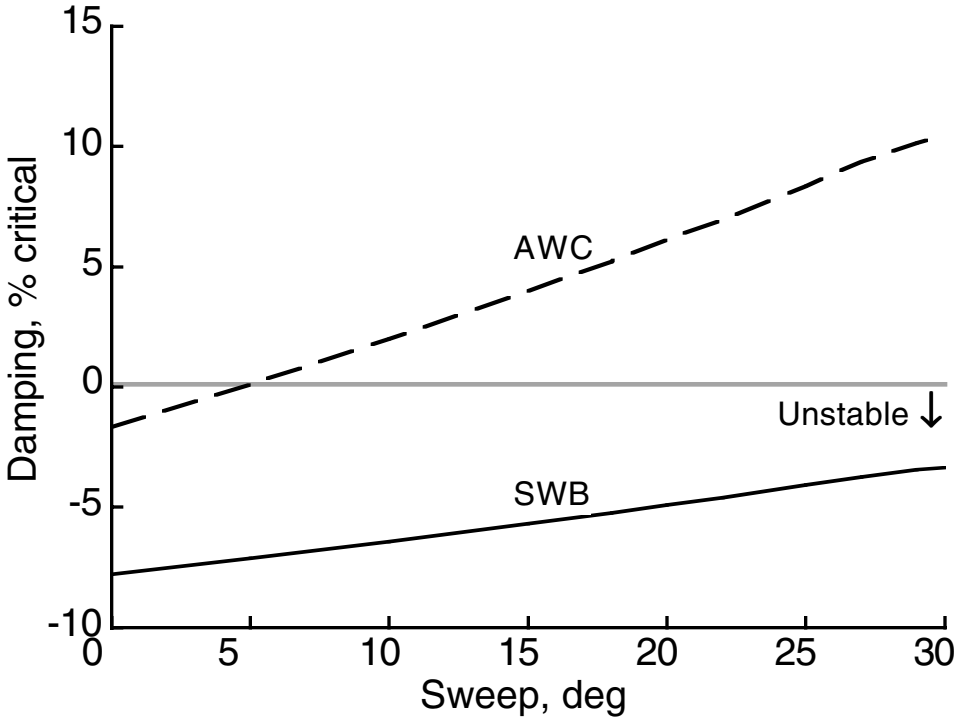

Figure 13. Variation of damping with tip-mass offset at 300 knots with –30 deg δ_3. Offset is calculated as equivalent sweep (see fig. 11(c)).

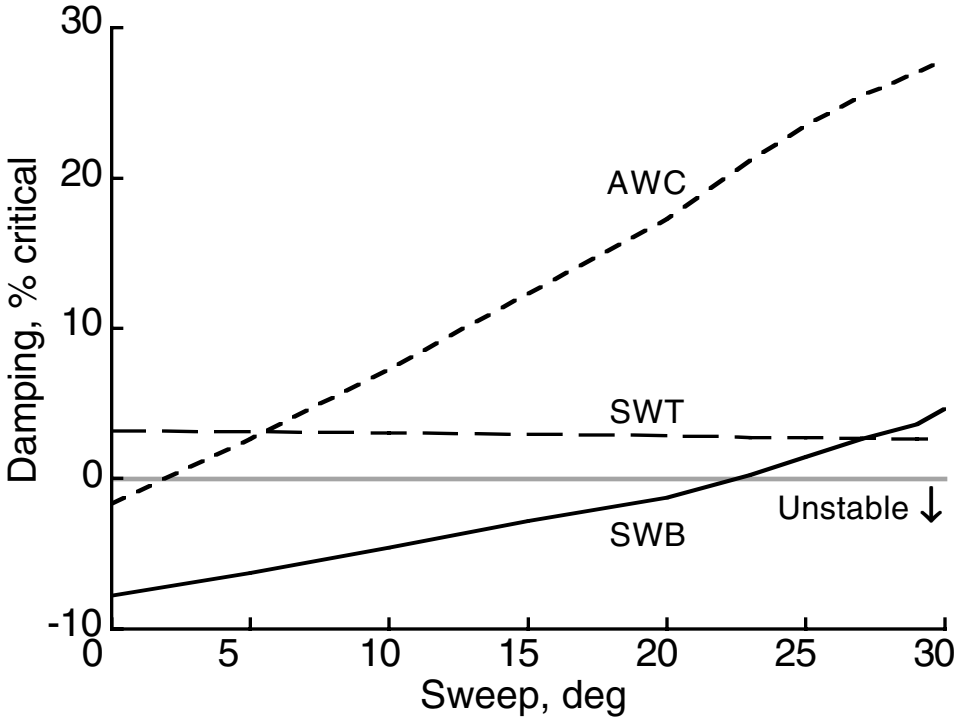

Figure 14. Variation of damping with combined sweep and tip-mass offset at 300 knots with –30 deg δ_3. Offset is calculated as equivalent sweep (see fig. 11(e)).

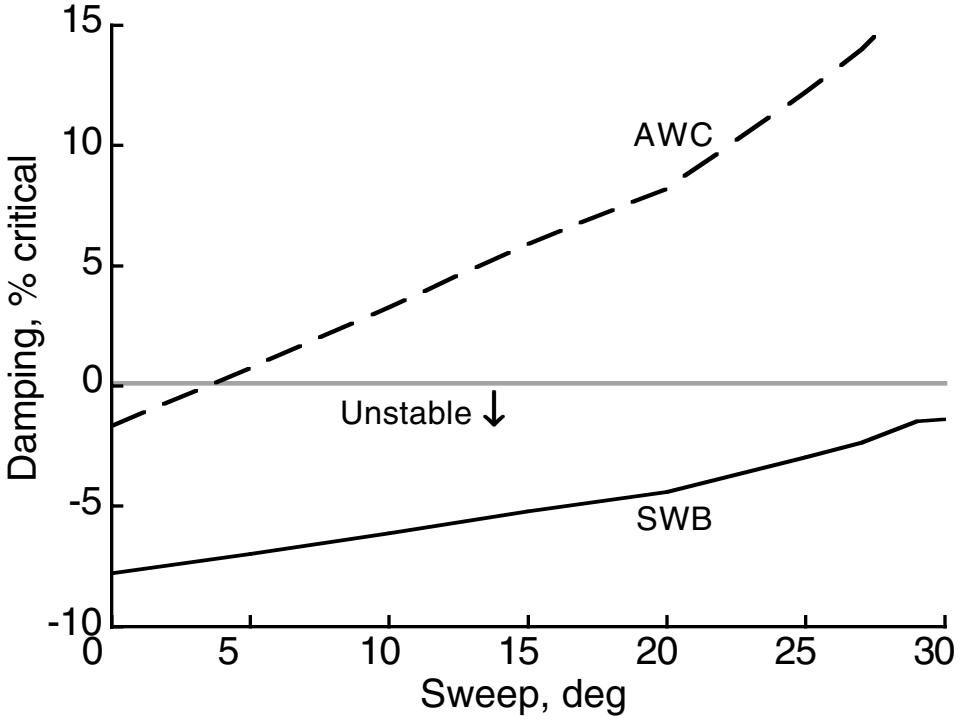

Figure 15. Variation of damping with sweep and fixed tip-mass position at 300 knots with –30 deg δ_3. Offset is calculated as equivalent sweep (see fig. 11(d)).

A more practical approach is to move the tip mass inboard, so that it is fully enclosed in the airfoil (suggested by David A. Popelka). For the predictions of figure 16, the entire tip mass was moved to 0.8R (the beginning of sweep) and positioned at the leading edge. The amount of mass was also doubled. (With the standard weight, the predictions were closely similar to those of fig. 15.) The SWB mode now becomes stable at 23-deg sweep. Because the SWT mode decreases slightly with sweep, the optimum value of sweep is 29 deg.

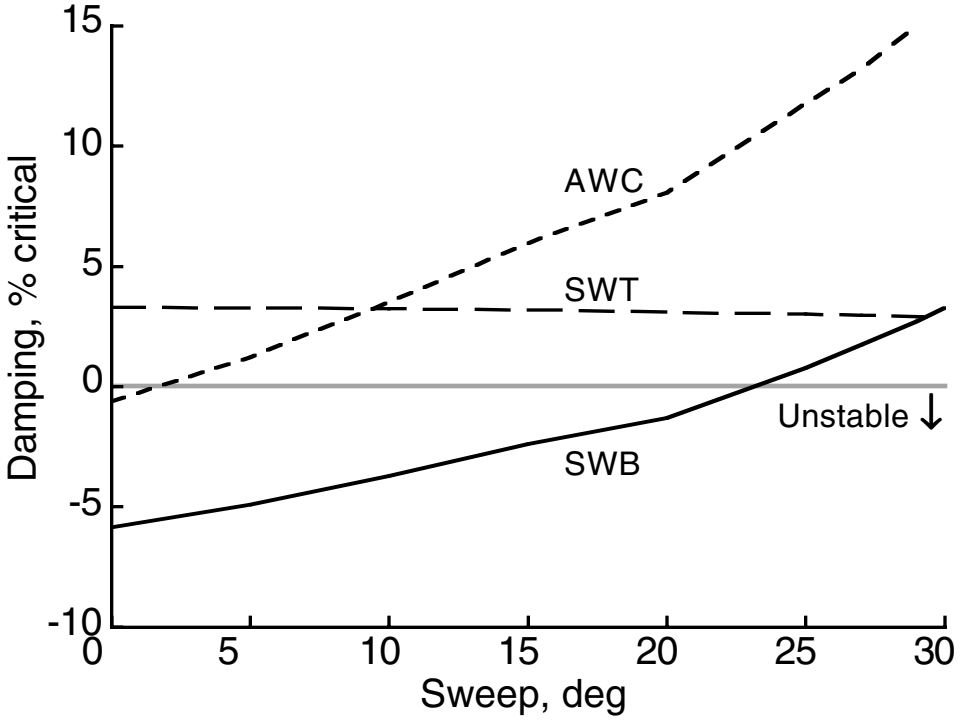

Figure 16. Variation of damping with sweep for double tip mass at inboard position at 300 knots with –30 deg δ_3 (see fig. 11(f)).

For ease of comparison, figure 17 replots the predictions for SWB mode damping. It emphasizes the effects of mass offset on the sensitivity of damping to sweep and on the nonlinearity of the responses. An offset tip mass would have to be placed on a boom extending from the leading edge, or at least a large fairing. An inboard mass at the leading edge is nearly as effective as a tip mass on a boom.

Quasi-Static Couplings

Figure 18 schematically illustrates how sweep and mass offset alter the perturbational forces on the blade. A swept tip moves the center of pressure aft of the pitch axis, creating a favorable (nose-down) moment for perturbational lift. An offset tip mass has an inertial reaction force ahead of the pitch axis, again creating a favorable moment. The blade mode shapes will be different for the two cases, leading to different net effects on stability.

Figure 19 shows the quasi-static modal coupling ratios for sweep and mass offsets, corresponding to figures 11(b) and 11(c). For sweep, the pitch/lag coupling is always favorable (lag back, pitch down), but pitch/flap coupling is unfavorable. For the range of sweep angles considered here, the pitch/flap coupling is never negative, but the slope becomes favorable above about 20-deg sweep, helping to explain the nonlinear variations of figure 12. For tip-mass offsets, both couplings are always favorable, but much more so for pitch/flap than pitch/lag.

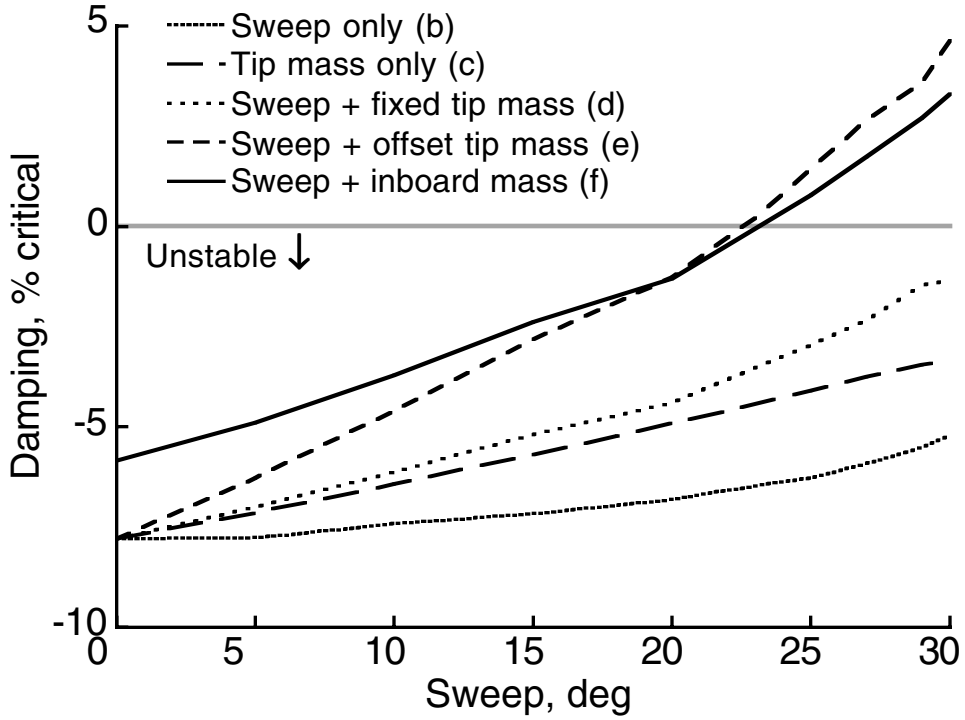

Figure 17. Comparison of the effects of sweep and mass offset on the SWB mode at 300 knots with –30 deg δ_3 (see fig. 11(e)). Offset is calculated as equivalent sweep (see fig. 11(c)).

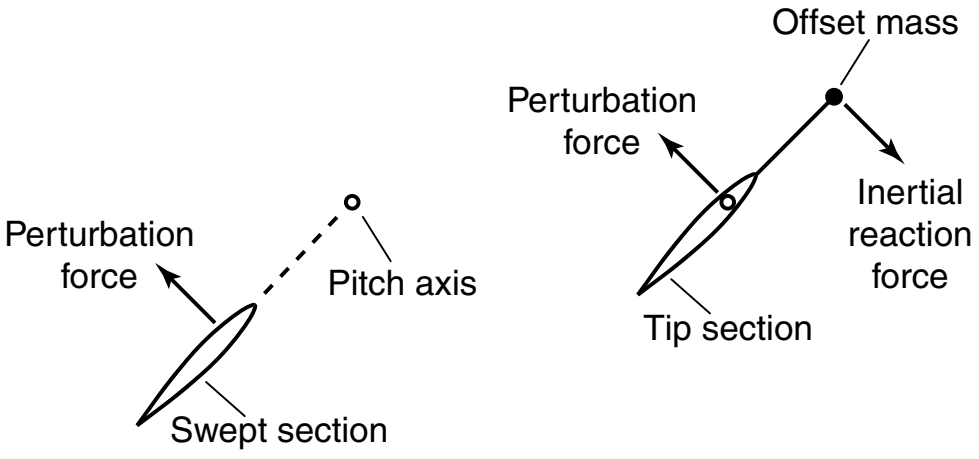

Figure 18. Perturbation and inertial forces on a swept section and an offset mass, respectively.

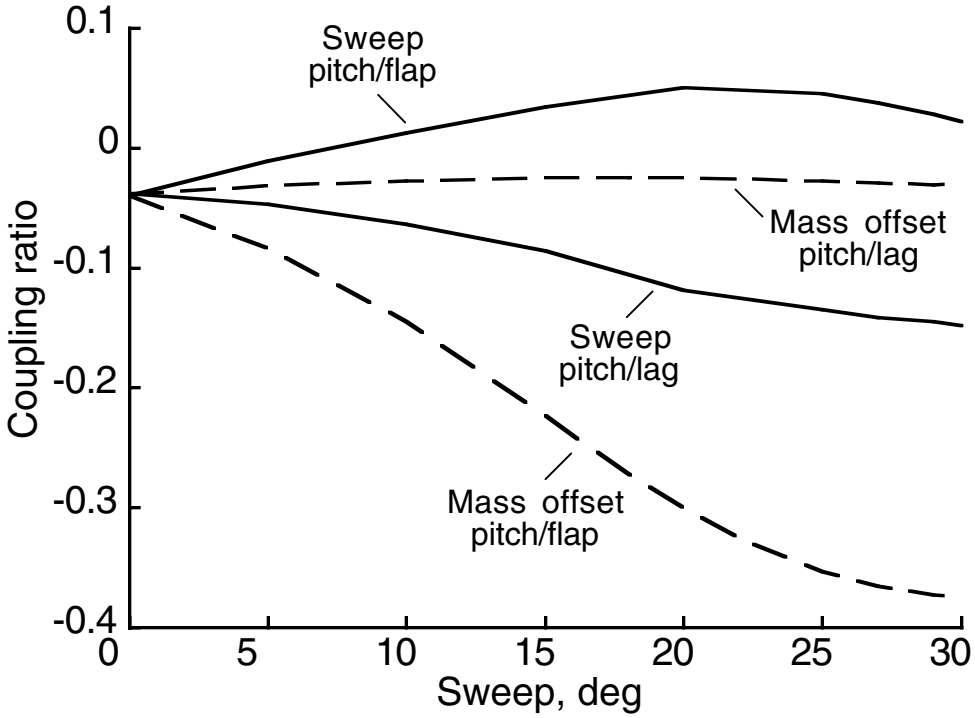

Figure 19. Modal coupling ratios for blade sweep and tip-mass offsets (Figs. 11(b) and 11(c) configurations).

Aerodynamic Effects

CAMRAD II can separately model various aerodynamic and structural features, two of which are examined in more detail here: aerodynamic sweep versus offset, and unsteady-flow effects. The aerodynamic panels can be swept independently of the structure, and the effects of offset can be calculated independently of the effects of sweep angle. Figure 20 schematically illustrates the difference between panel offset and panel angle. The aerodynamic collocation points are centered spanwise on each aerodynamic panel. Only four collocation points (at 1/4-chord) and two swept panels are shown in the figure; the V-22 model used here has 17 total aerodynamic panels, 6 of which are swept.

Figure 21 shows the effects on the SWB model of aerodynamic sweep only (no structural or mass sweep), panel sweep angle only (no offset), and full sweep without panel angles; the nominal full-sweep predictions (fig. 12) are repeated for reference. Stability was also calculated for aerodynamic offset only (no structural sweep or aerodynamic panel angle), but even at this expanded scale, the curve is nearly indistinguishable from the aerodynamic-sweep-only curve in figure 21 and so is not shown. It is clear that the effects of sweep on stability are dominated by the offsets of the aerodynamic panels, not by the angles of the panels. For reference, the maximum section Mach number at this speed is 0.7668.

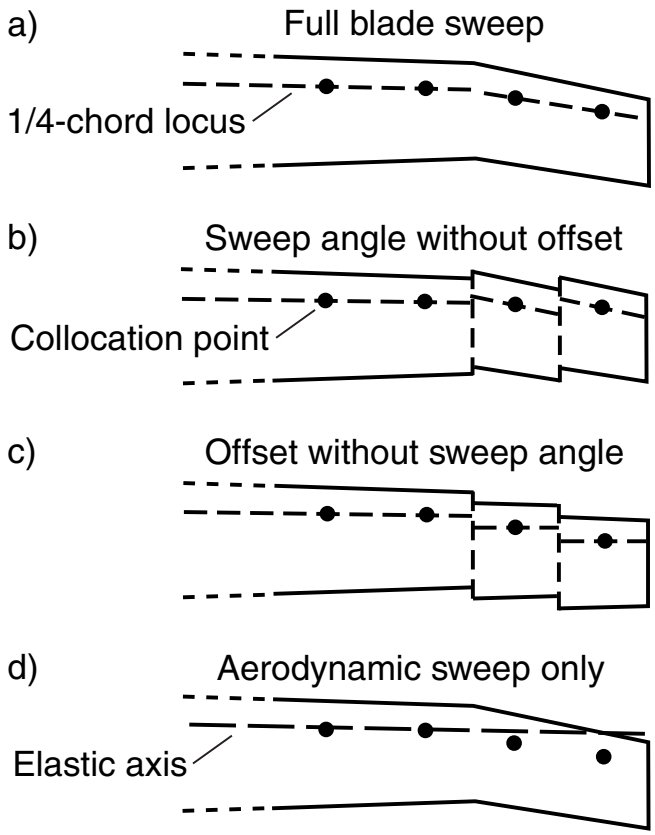

Figure 20. Differences between blade sweep, aerodynamic sweep, aerodynamic panel sweep angle, and aerodynamic panel sweep offset (compare with fig. 11).

Further insight can be drawn from figures 17 and 21. Blade anhedral has been shown to improve whirl-flutter stability (ref. 18). However, anhedral will include a mass offset, or droop, with respect to the tip path plane. Mass droop is equivalent to reduced precone and will be constrained by loads in hover and low-speed flight.

Because of the large change in collective angle between hover and airplane mode, the effective net mass droop will change significantly between flight modes. This will increase effective precone in hover and decrease it in airplane mode, thereby alleviating the problem. In figure 17, tip-mass offset is clearly stabilizing, even though the offset has a geometric component in the opposite direction to droop. Moreover, aerodynamic sweep without structural sweep is highly stabilizing (fig. 21), and it has no mass droop by definition. The beneficial effects of sweep cannot be explained by effective mass droop.

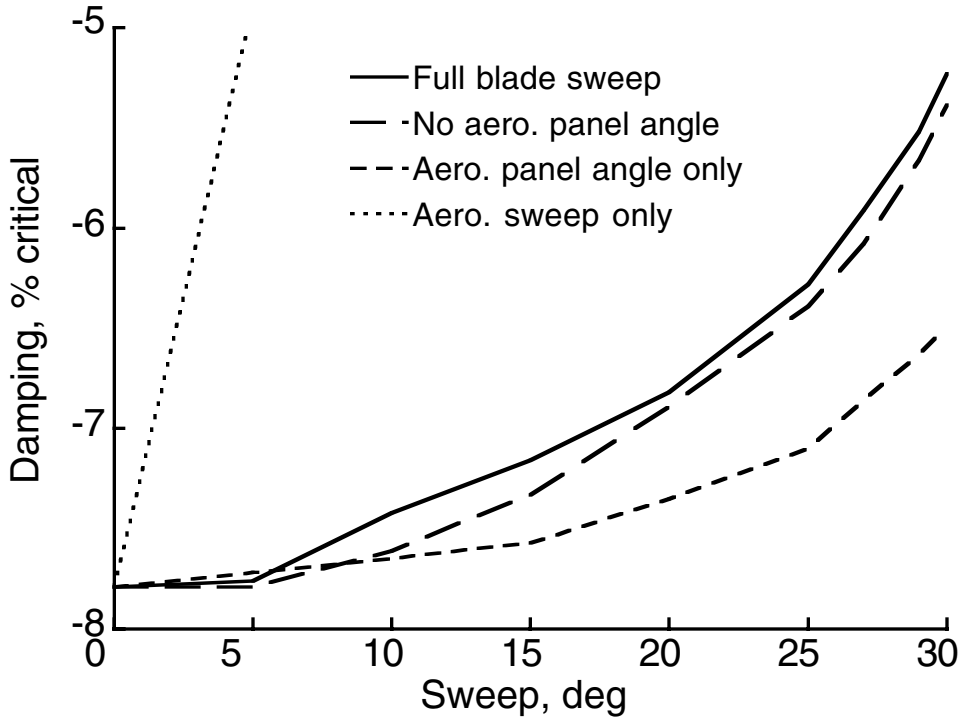

Figure 21. Comparison of the effects of aerodynamic displacement vs. angle on the SWB mode at 300 knots with –30 deg δ_3.

The effects of unsteady aerodynamics were important for some modes. The most dramatic example is shown in figure 22, for the SWB mode. This figure also shows the full effect on stability of idealized aerodynamic offset (no panel sweep or structural offset, fig. 20(c)), which runs off the scale of figure 21. This idealized model is more sensitive to the effects of panel angle and unsteady aerodynamics than the full model, making the effects easier to discern in the plot. The curve for full aerodynamic sweep (with panel sweep but no structural sweep, fig. 20(d)) is also shown; as in figure 22, the local sweep of the panels makes little difference.

Figure 22 shows that unsteady aerodynamics reduce stability for low and moderate values of offset, but for large offset, unsteady effects greatly increase stability. With full blade sweep (not shown), elimination of unsteady aerodynamics shifts the damping curves up with little change in trends with sweep. Significant effects were also seen for the least stable antisymmetric mode (AWC) and for tip-mass offsets (not shown). In such cases, the trendlines were again simply shifted up a few percent when unsteady effects were removed, so that there was little effect on the sensitivity of stability to sweep or offset.

Although unsteady aerodynamics clearly affect stability, they are not the dominant mechanism behind the beneficial effects of sweep. Because unsteady aerodynamics have their greatest effect on the largest values of aerodynamic offset, which are already highly idealized design variations, unsteady effects could have been ignored without invalidating the analyses of other configurations. Nevertheless, unsteady aerodynamic effects were retained for all analyses reported here, excepting only those shown in figure 22.

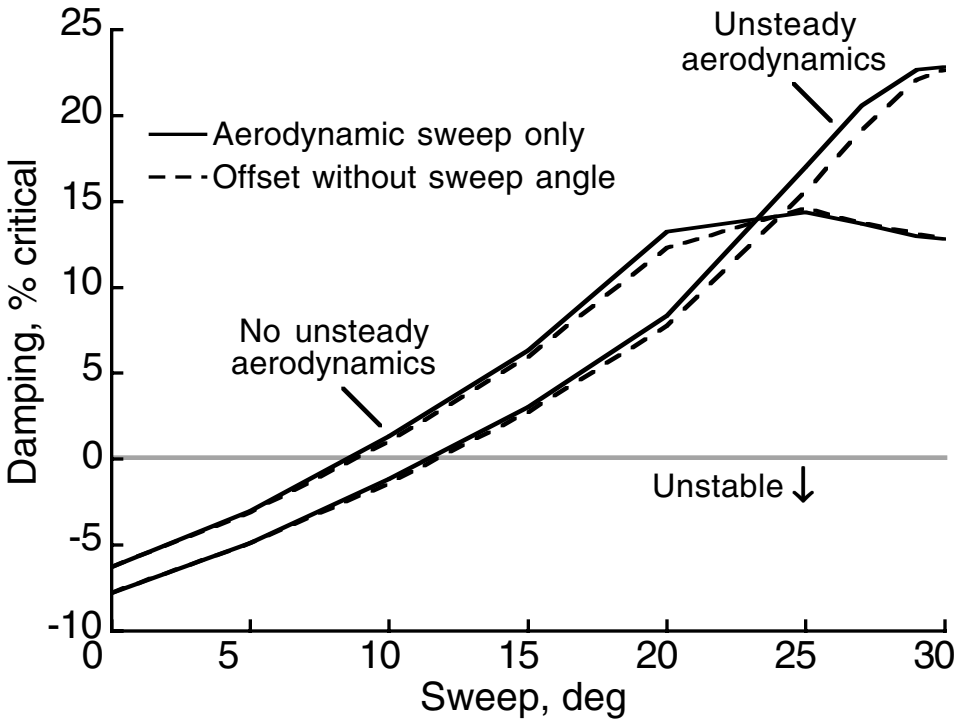

Figure 22. Effects of aerodynamic displacement on the SWB mode, with and without unsteady aerodynamics, at 300 knots with –30 deg δ_3.

A Practical Example

Several of the design variations covered so far are impractical, even physically impossible. One of the more effective and practical configurations, sweep with inboard tuning mass (fig. 11(f)), was chosen for further study. The intention is to examine the blade mode shapes for insight into the mechanism by which sweep and mass offsets affect whirl-mode stability. With pure blade sweep, as in figure 11(b), the tip mass is moved in the wrong direction for stability. If the mass is placed sufficiently inboard, it is unaffected by sweep, as in figure 11(f). Such a design makes the effects of sweep on the blade mode shapes more evident, as illustrated in the following discussion.

In order to focus attention on the key blade modes, the number of modes was systematically reduced until the stability trendlines for the SWB whirl mode showed significant departures from the full model (fig. 23). The minimum number of blade modes was thereby determined to be four: the first flap and lag modes, the rigid pitch mode, and the second flap mode.

For SWB, the model with only four blade modes closely reproduced the trends of stability with sweep (fig. 23), but with a slight offset. For AWC, the match was not as good, but because AWC is always more stable than SWB, and usually much more so, the simple model is adequate.

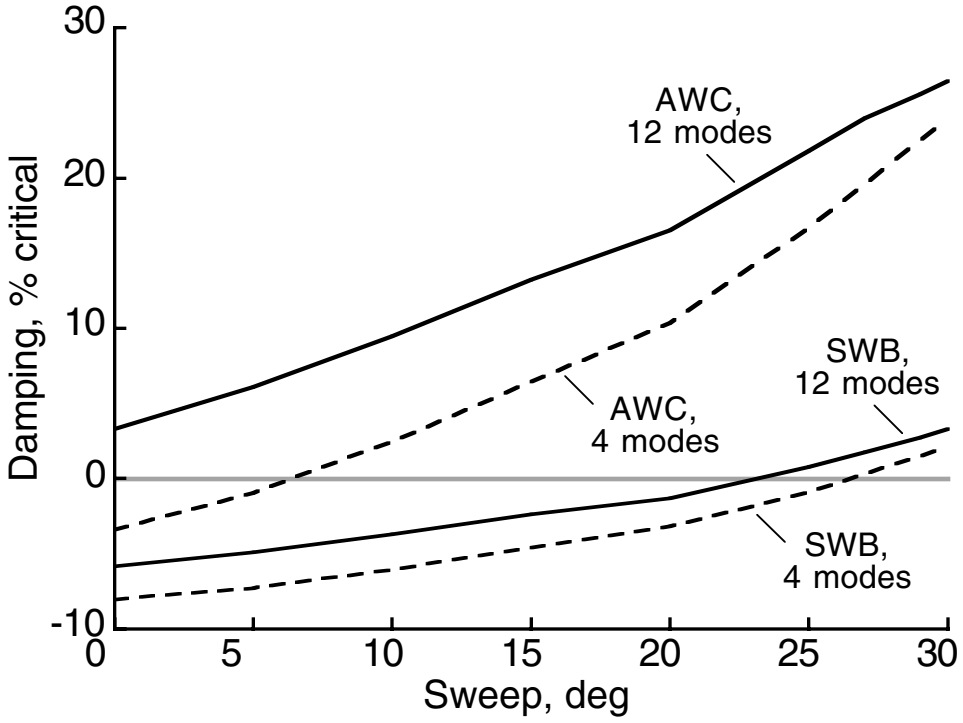

Figure 23. Effects of simplified dynamic model on the most sensitive modes, for sweep with inboard tuning mass at 300 knots with –30 deg δ_3.

Adding the first elastic torsion mode (the seventh mode in order of frequency) brought the predictions into much closer agreement with the full model, but only by shifting the curves upward without appreciably changing the trends. Moreover, the elastic torsion mode shapes were little affected by sweep. Although this indicates that the elastic torsion mode is essential for accurately predicting stability boundaries, it also implies that this mode is not important for explaining the physical mechanisms by which sweep affects stability.

Normalized mode shapes are plotted for the uncoupled blade modes at 332 rpm, as shown in figures 24–28. Only the four modes in the simplified model are shown. The figures also show the changes in the torsion mode shapes as sweep is varied in increments of 5 deg. Displacements (flap and lag) are scaled in feet; rotations (pitch/torsion) are scaled in radians. Flap is perpendicular to the hub plane (not the local beam axis), positive up (or forward, in airplane mode); lag is in the hub plane, positive aft (against the direction of rotation). Pitch/torsion mode shapes are positive nose up. The trimmed pitch angle at 0.75 R was 43 deg for 0-deg sweep.

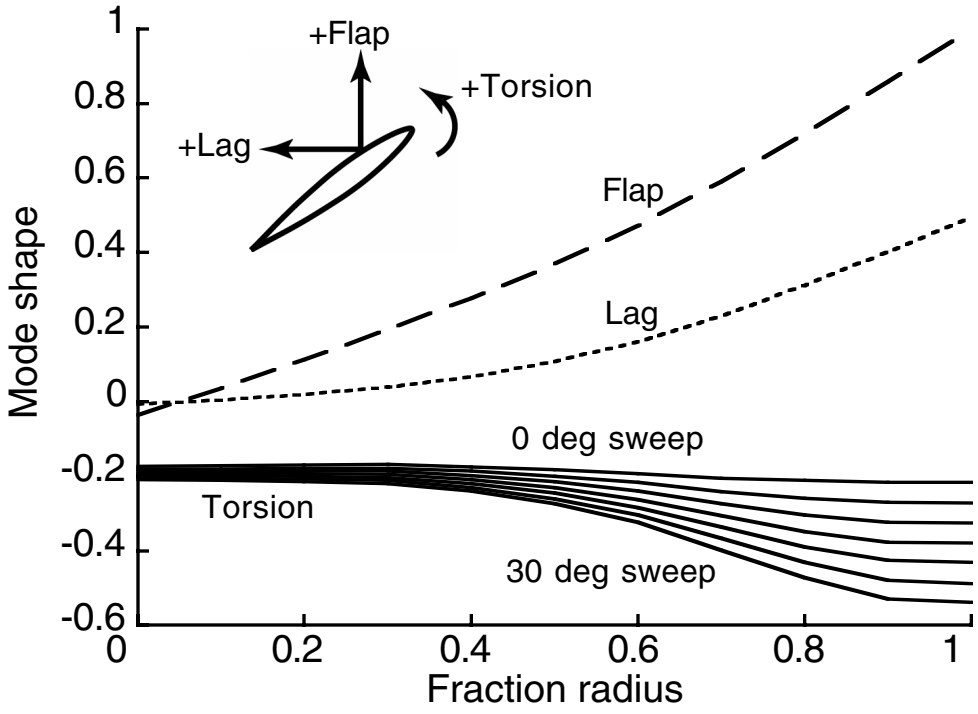

Figure 24. Mode shapes for the first flap mode.

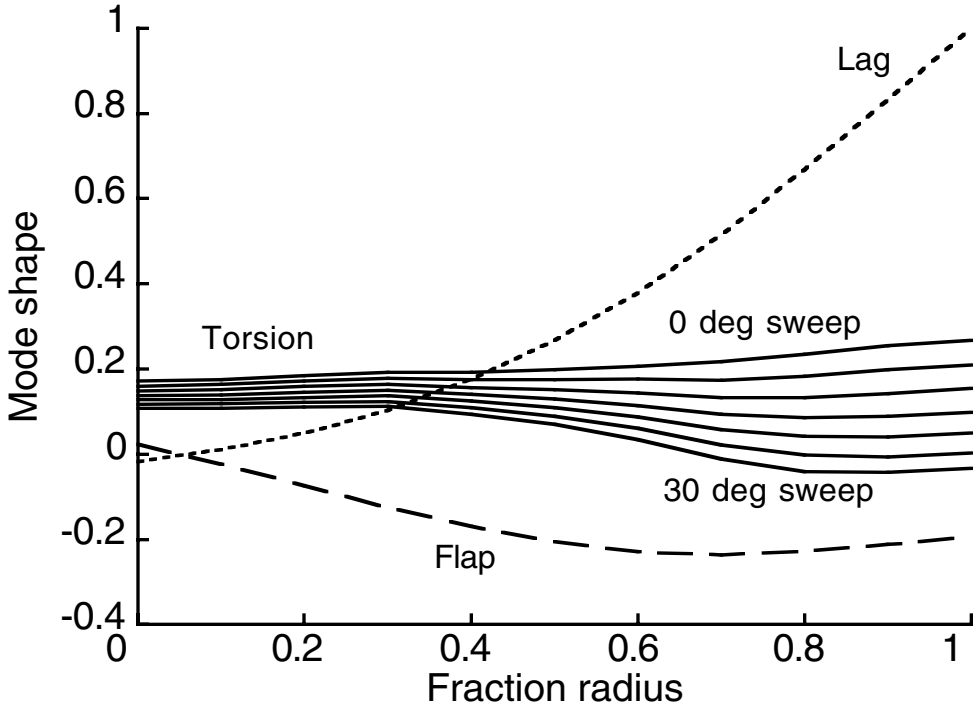

Figure 25. Mode shapes for the first lag mode.

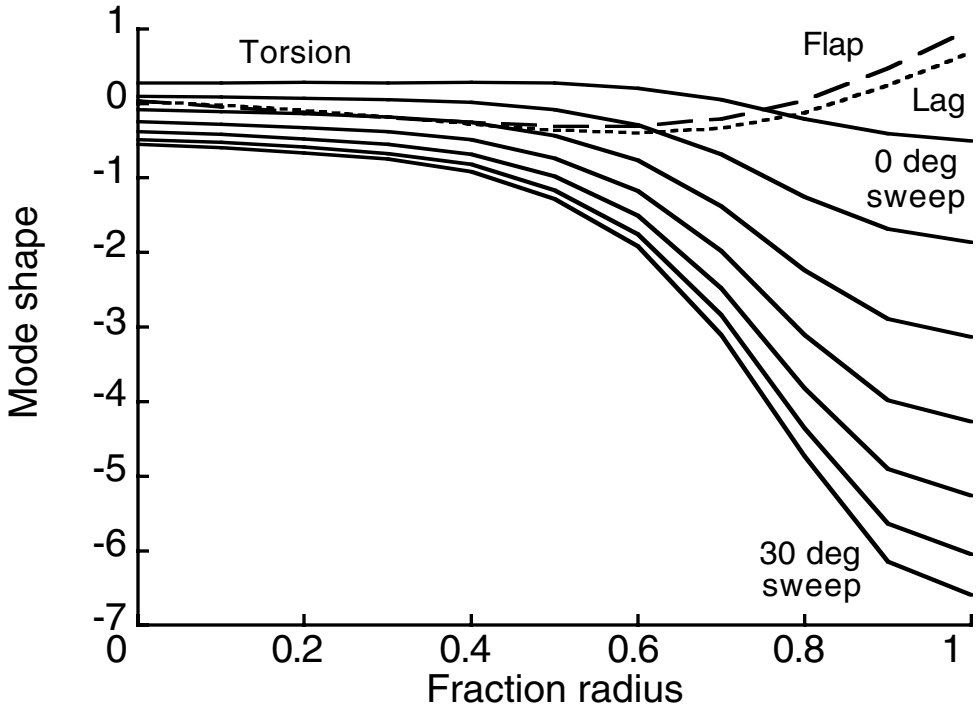

Figure 26. Mode shapes for the second flap mode.

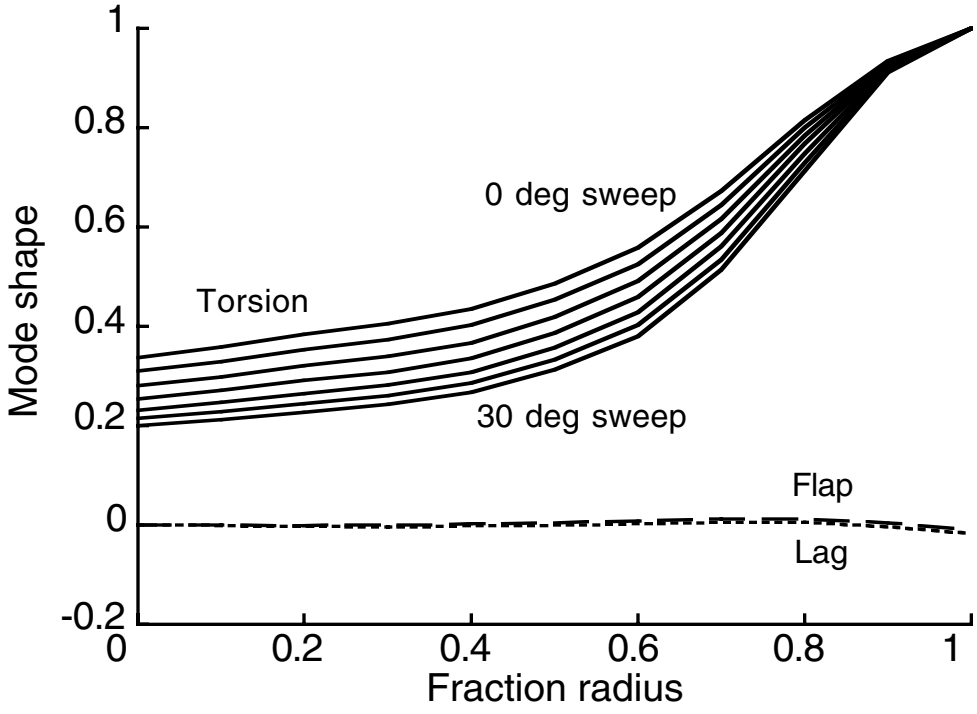

Figure 27. Mode shapes for the first pitch/torsion mode, referenced to the blade tip.

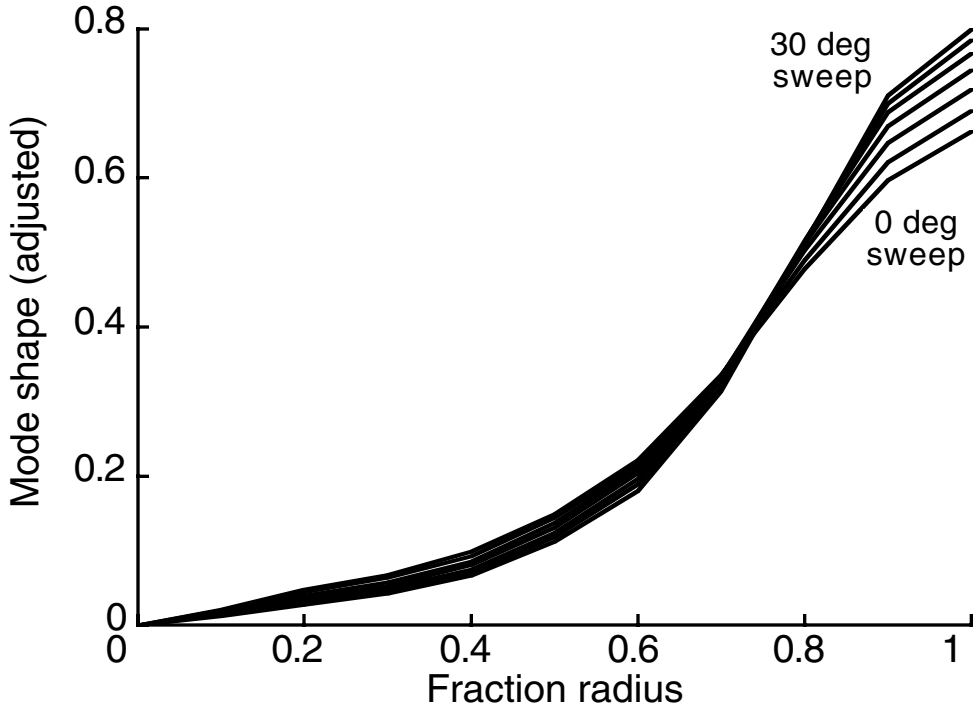

Figure 28. Torsion mode shape for the 1st pitch/torsion mode, offset to force zero values at the root for all values of sweep.

For the modes shown here, flap and lag mode shapes were little affected by sweep. The differences are difficult, if not impossible, to discern at the scale of figures 24–28. For the sake of legibility, flap and lag mode shapes are shown only for 0-deg sweep. In figure 28, the curves are offset to have zero displacement at zero radius for all sweep angles.

Figure 29 shows the uncoupled blade mode frequencies at 332 rpm, plotted against sweep. The first flap and lag frequencies, at 1.22 Hz and 1.34 Hz, respectively, vary only in the fourth decimal place and are not shown.

At the trimmed flight condition—300 knots, 332 rpm, and 7500-ft altitude—the blade pitch angle at the tip is just over 35 deg. The mode shape of the first flap mode (fig. 24) is almost perpendicular to the local chord at the tip. As sweep is increased, there is an increasingly negative torsional component. The associated reduction in local lift reduces the flapping motion and so stabilizes the mode. Similar effects can be readily deduced for the other flap/lag modes by inspection of figures 25 and 26.

It will be obvious that sweep helps to stabilize pitch/torsion modes by creating a counteracting aerodynamic moment for any torsional perturbation. Figure 27 suggests that sweep also changes the mode shape so as to enhance this effect. This can be better understood if the shapes of the first pitch/torsion mode are replotted as in figure 28, which better represents the physical behavior of the blade. For any given amount of torsion mode deflection, increasing sweep increases the effective pitch deflection at the tip, where the dynamic pressure is highest, thereby increasing the stabilizing moment.

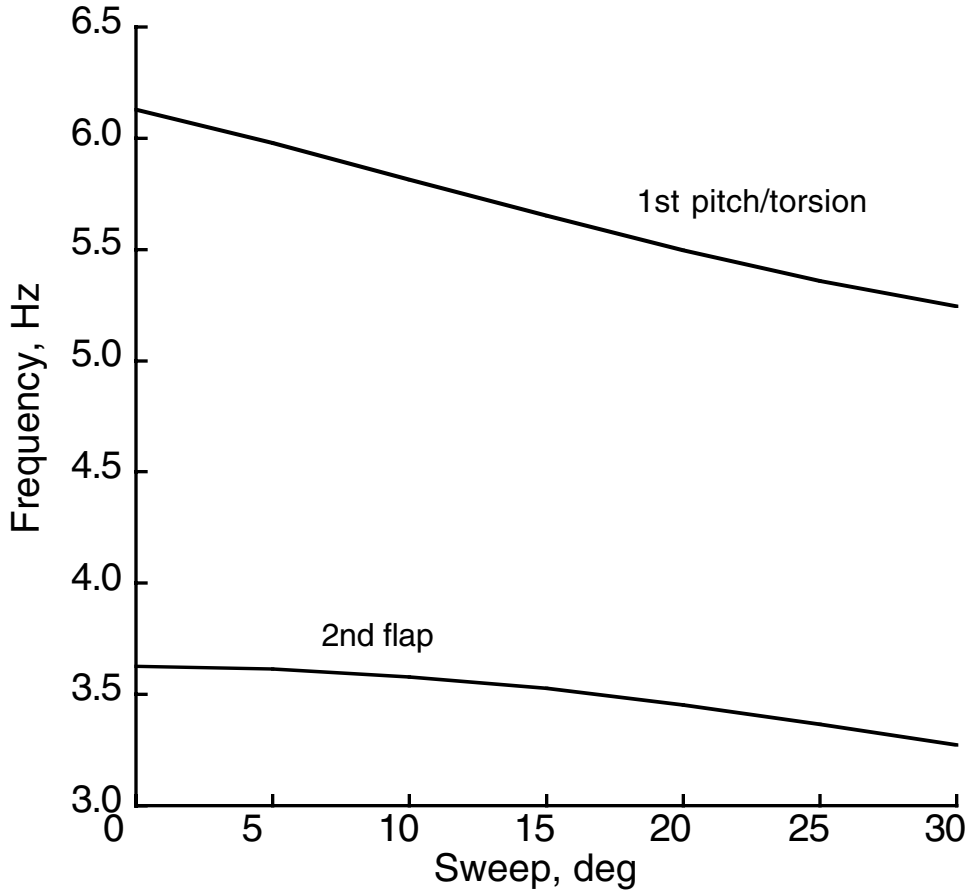

Figure 29. Modal frequency variations with sweep.

These effects of sweep and mass offset on aeroelastic stability are directly analogous to those for swept, fixed wings, although here much complicated by the existence of a pitch mechanism and control-system flexibility, a gimbal and associated pitch/flap kinematics (δ_3), a flexible drive train, and the dynamics of the coupled rotating system. Their effects on whirl flutter are, of course, determined by the coupling between the fixed and rotating systems.

Modal Coupling Effects

As shown by Gaffey (ref. 17), flap-lag stability at high inflow requires positive pitch/flap coupling (negative δ_3) between the blade and control system. However, figures 24 and 26 imply that sweep and mass offset stabilize the rotor by introducing negative pitch/flap coupling. The apparent contradiction can be resolved by the following observations:

A major contribution to whirl-mode instability is the out-of-plane component of the first lag mode (fig. 25), which couples the lag mode to control-system kinematics. The slopes of the flap and lag mode shapes have opposite sign at the root, reversing the effective coupling. For positive δ_3, the net coupling is lag back, pitch up, which is destabilizing. At high inflow, the rotor is very sensitive to this effect (ref. 17), and negative δ_3 is needed to stabilize the rotor. The values of sweep and mass offset examined here have little effect on the flap

and lag mode shapes; indeed, the changes near the root are impossible to discern at the scale of figures 24–27. Therefore, the beneficial control-system couplings are unaffected.

For the lag mode (fig. 25), sweep changes a mild, positive pitch/lag coupling to a stronger, negative pitch/lag coupling, which is stabilizing. Note also that the changes in pitch/torsion mode shapes are seen much more strongly at the tip than at the root (although fig. 27 suffers from the normalization method used by CAMRAD II; fig. 28 is more revealing).

The stabilizing effect of negative δ_3 is seen as favorable shifts in the first flap and lag frequencies, which decouple the modes (ref. 17). Sweep and mass offsets have negligible effects on these frequencies: the largest change seen here was less than 1%. Therefore, the frequency separation is unaffected.

To summarize, for a rotor with a swept tip, the benefits of positive pitch/flap coupling at the root are retained for the rotor as a whole, while the benefits of negative pitch/flap coupling are realized near the tip, where the dynamic pressure is greatest.

LOADS

The effects of rotor modifications on loads were investigated to check for potentially serious changes. Table 1 summarizes the flight conditions analyzed. All conditions analyzed were derived from flight test data in reference 19, but they do not necessarily match any particular test condition. All conditions except cruise were analyzed at sea level, with a rotor speed of 397 rpm. The cruise condition was 15,000 ft and 333 rpm.

Table 1. V-22 flight conditions for loads analyses.

Flight mode	Pylon angle, deg	Airspeed, KTAS	Power, SHP
Hover	90	0	7050
Helicopter	85	60	3860
Conversion	75	80	3750
Conversion	60	100	4350
Conversion	30	140	4470
Cruise	0	275	7660

Loads were calculated with a multiple-trailer free-wake model derived from that of reference 9. For trim, each blade had 12 dynamic modes (not just static deflections, as in the flutter analyses), and the rotor response was calculated with 10 harmonics. See the appendix for details.

Ideally, the loads analysis would use a complete model of the airframe aerodynamics and control system, with different aerodynamics and control phasing for each pylon angle and flap setting. However, no such models have yet been developed for the V-22 using CAMRAD II. Fortunately, the changes of interest apply only to the rotors, so an isolated rotor model is adequate. It also saves considerable computational time—a nontrivial issue with a free-wake model.

For all loads analyses, the isolated rotor was trimmed to zero flapping (zero gimbal tilt). Although this does not exactly match flight conditions, it is adequate to identify significant changes to loads and performance

caused by blade sweep and other design modifications. It also establishes a more consistent rotor trim for all flight conditions, facilitating comparisons. There are thus four linked trim parameters: pylon angle, input as rotor shaft angle of attack; airspeed; rotor speed; and rotor power, input as one-half the total power in table 1.

Because critical trim parameters were varied together, the trends of loads with airspeed or any other parameter should not be expected to be smooth or even monotonic. The data are plotted here as connected data points to simplify the figures and improve legibility. Caution should be exercised when attempting to interpret any apparent trends with airspeed.

Loads were calculated for the pitch links, grip (0.05 R), yoke (0.05 R), and blade (0.35 R); in-plane (lag) and out-of-plane (flap) loads were calculated at each location (except the pitch links). Steady and vibratory loads were calculated as mean and half peak-to-peak (hpp) values.

Loads were calculated and compared for two rotors: the baseline V-22 rotor, and a rotor with 30-deg blade sweep and inboard tuning weights (the same rotor as in figs. 24–28, but only with the largest value of sweep). Only the most extreme differences are presented here. The swept rotor had a –30 deg δ_3 hub to match the stability calculations shown previously.

In order to prevent confounding the effects of rotor-blade design with the effects of δ_3, loads for the baseline rotor were also calculated with a –30 deg δ_3 hub. Changes in loads are therefore attributable only to changes in the blade design. The effects of design changes on loads are summarized in figures 30 and 31 for –30 deg δ_3.

Figure 30 plots the pitch-link loads against airspeed for the two blade designs. Compared to the baseline blade design, the mean pitch-link load for the swept rotor is increased by 19% at 275 knots. This was the largest increase seen for any load. The amount of change due to –30 deg δ_3 was only +0.1%.

Figure 31 plots blade lag loads (at 0.35 R) for the two blade designs. The half peak-to-peak loads varied very little and are not shown. The swept blades actually reduce the total load over most of the flight regime, and the worst-case load (about 4000 ft-lb at 50 knots) is about half the magnitude of the worst-case load for the baseline rotor. The load reduction at 275 knots is 88%. This is the largest absolute difference seen for any load. (The amount of change due to –30 deg δ_3 was only –4%.)

However, the large load reductions may be merely fortuitous: as shown in figure 31, both the inboard tuning mass (without sweep) and sweep with the nominal tip mass (fig. 11(b)) make the lag loads worse, but shifted in opposite directions relative to the baseline. The near-zero load at 275 knots may be only a coincidental canceling of the two effects. Nevertheless, the results are highly encouraging.

The effects on performance were also examined, using the same isolated-rotor model as was used for loads. Because the rotor was trimmed to power without an airframe aerodynamic model, figure of merit (at hover) and propeller efficiency (at 275 knots) were used for comparison. The differences were minor, but positive: compared to the baseline rotor (with –30 deg δ_3), the swept rotor improved figure of merit from 0.79 to 0.80 for M_{tip} = 0.709, C_T = 0.0137, and C_P = 0.00143; propeller efficiency improved from 0.84 to 0.85 for helical M_{tip} = 0.766, C_T = 0.00500, and C_P = 0.00418. The beneficial effects of sweep on performance at high Mach numbers (ref. 20) would not be expected to come fully into play at the airspeeds examined here. It is sufficient that there be no adverse effects, as was the case.

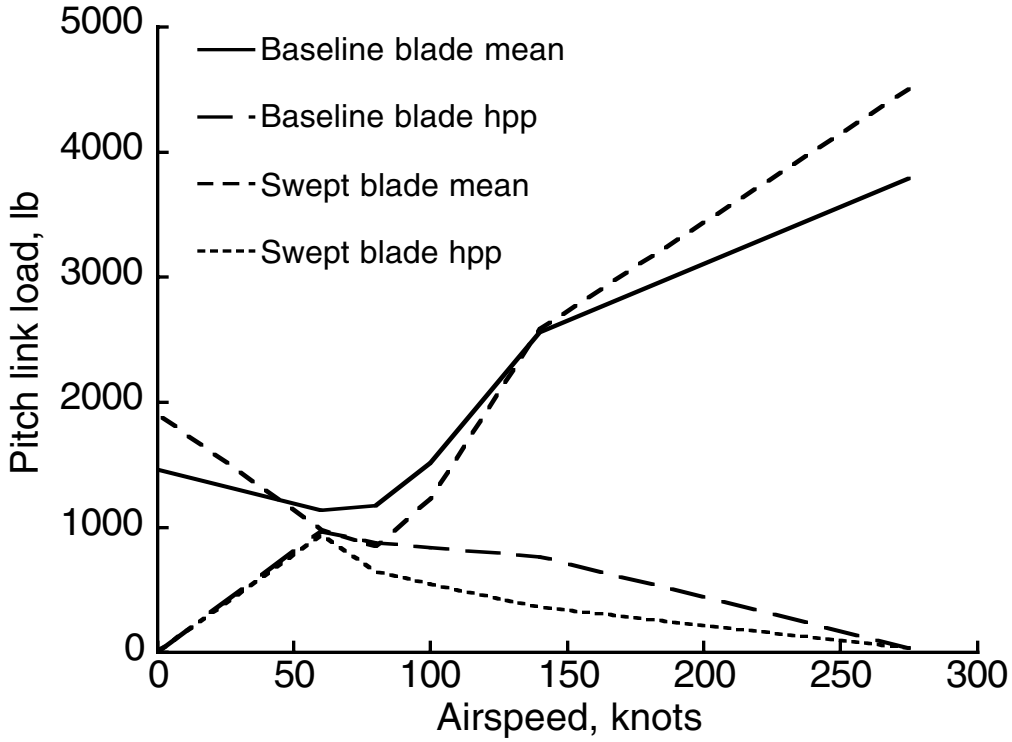

Figure 30. Pitch-link loads for the baseline and swept rotors.

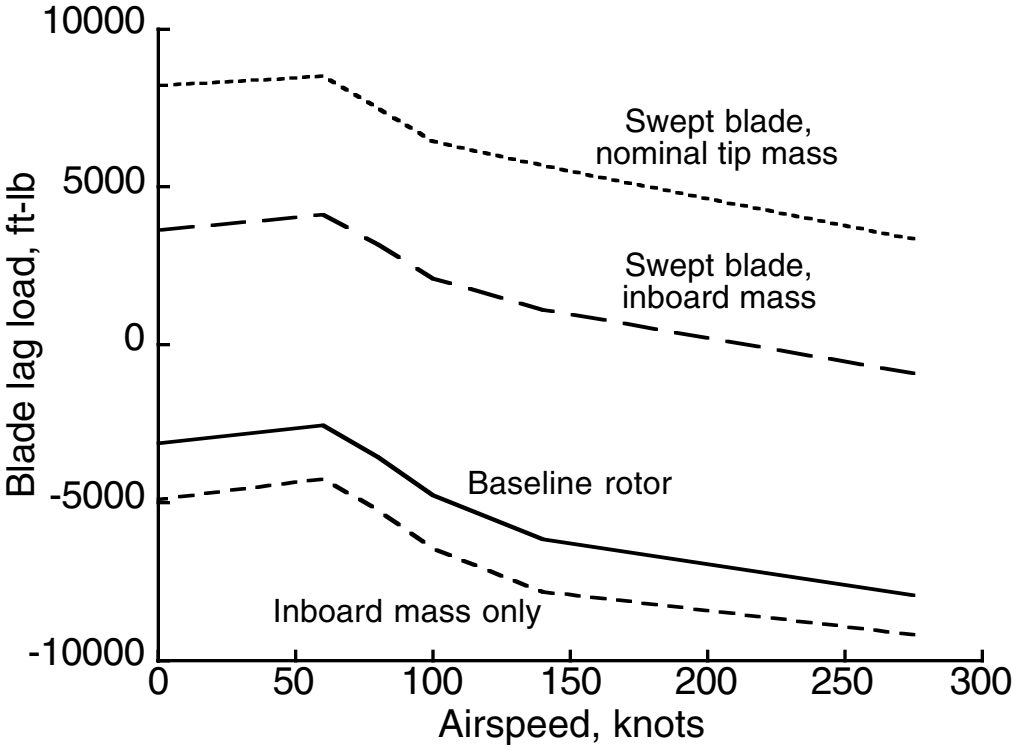

Figure 31. Mean blade lag loads for the baseline and swept rotors, and for an inboard tuning mass.

MODEL IMPROVEMENTS

Further efforts are recommended in three areas: research into the physical mechanisms by which sweep affects stability, improved designs to maximize stability, and further development of the V-22 CAMRAD II model.

Although the results presented here provide a plausible explanation of the role of mode shapes in enhancing the stability of swept-bladed rotors, the explanation is not definitive. The current rotor model is too complicated for efficient numerical examination of pitch/flap/lag coupling and other effects: too many modes are required, both for the rotor and for the airframe, to adequately characterize the system response. Direct examination of the flutter matrices or the eigenvectors is appropriate, but would require much smaller matrices, hence a much simpler model, to be practical.

The relative contributions of aerodynamic and inertial effects were only inferred, not directly calculated. Also, sweep and mass offsets were always in the local chord plane, so there was no direct examination of the relative effects of sweep versus mass droop. These effects may all be expected to interact with each other.

It is fundamentally difficult to separate the relative contributions of the different elastic deformations and couplings. Even for an unmodified rotor, blade elasticity is intimately involved in whirl-mode instability in the first place. Therefore, the effects of blade elasticity cannot be fully decoupled from those of sweep. Similarly, the effects of tip-mass inertia cannot be studied in isolation without changing the underlying aeroelastic phenomena being explored. However, such effects can be inferred from parametric blade-design studies, such as those presented here. The present V-22 model does not lend itself to efficient exploration by such methods, so a new model is being developed specifically to support further studies of whirl flutter. It need not be as accurate as the model used here, as long as it captures the general features of V-22 behavior.

Even without further insight into the physical mechanisms, improvements in blade design should be possible with conventional optimization techniques. Although true optimization is beyond the scope of the present research effort, a few initial steps would be helpful to guide further efforts. In particular, it should be straightforward to determine the tradeoff between the local amount of sweep versus the radial extent of sweep, and whether sweep should be in the local chord plane or in some other direction. Efforts should also be made to determine whether aeroelastic tailoring can be combined with sweep to increase favorable torsional components of the flap/lag modes. More comprehensive loads analyses are obviously warranted as part of any design studies.

There are several possible areas of improvement for the CAMRAD II model of the V-22 rotor: details of the grip/yoke model, more sophisticated control-system kinematics, and improved aerodynamics models. A few examples are discussed here.

The coupled swashplate model is not exact. Ideally, the extension and rotational (i.e., collective and cyclic) mode shapes should be taken at the transmission adapter, but the transverse mode shapes should be taken from the hub, or if possible from the actual trimmed swashplate location. Another approach would be to explicitly model the nonrotating actuators. Although the kinematic differences would be small, the high sensitivity of whirl-mode damping to control-system kinematics suggests that such an improved model is worth pursuing.

The C81 tables are a major limitation for stability analyses. The area of concern is limited to very high speeds, so the effects on the present research are thought to be negligible. However, establishment of reliable

stability trends at high speeds is still desirable and could benefit from improved aerodynamic tables. The key requirement is to generate coefficient data at Mach number increments small enough to guarantee that all significant nonlinear variations are captured. Recent CFD methodology (ref. 21) promises to significantly improve the aerodynamic models needed for whirl-mode predictions.

Very little attention was paid to airframe aerodynamics during this research. It is largely irrelevant for power-off stability, and the existing wing-body aerodynamic tables are adequate for power-on whirl-flutter analyses (ref. 11). Obvious avenues for future improvements are to generate a comprehensive set of CAMRAD II wing-body tables, or possibly to update the coefficients used by the internal aerodynamic model. Such models will eventually be needed for loads analyses.

CONCLUDING REMARKS

The V-22 was analyzed with CAMRAD II to evaluate whirl flutter in airplane-mode flight. The effects of blade sweep and tip-mass offsets on whirl-flutter stability were examined. The rotor was (analytically) destabilized by increasing the magnitude of kinematic pitch-flap coupling (δ_3) to –30 deg. Different combinations of blade sweep and mass offset were evaluated; the most favorable combinations greatly increased the damping of the least stable modes, more than enough to fully stabilize the rotor.

Configurations examined included sweeping the outer 20% of the blade aft a maximum of 30 deg (about one chord length), moving the tip balance weight forward up to the same equivalent offset, and moving the tip weight inboard of the swept section. A combination of 30-deg sweep with an inboard tuning mass represented a practical and effective design; this rotor was stable with –30 deg δ_3. A simple survey of pitch-link loads indicated an increase of 19% (mean steady load) at high speed, and lag loads were substantially reduced. It should, therefore, be possible to achieve a significant increase in whirl-mode stability combined with decreased lag loads, with an acceptable increase in pitch-link loads.

Several possible mechanisms were examined for their effects on whirl-mode stability. Tip-mass offsets increase the inertial coupling about the pitch axis in response to perturbational forces. Tip sweep enhances the torsional components of blade mode shapes, increasing favorable aerodynamic couplings. Both effects reduce the V-22 blade response to destabilizing perturbations. Sweep also alters the unsteady loads, but this effect is of lesser importance for increasing stability. The reduction of local lift-curve slope caused by sweep has little effect on stability.

APPENDIX

EXAMPLE JOBS WITH WAKE MODELS

Example CAMRAD II job files used for loads and performance calculations are listed in this appendix. They are intended for use with the V-22 model documented in reference 10. Note that the examples given here are for an isolated rotor, which is a subset of the model in reference 10.

Three wake models are included: a multiple-trailer model for edgewise flight, and two axial-flow models, one for hover and one for high-speed cruise. The axial-flow models differ by only one line of code, which is commented out in the example job. These models also include inboard stall delay for better performance prediction (ref. 22). The full rotor aerodynamics namelist is included to show its relationship to the stall-delay model.

The first example is a multiple-trailer job for 30-deg nacelle angle at 140 knots (slightly simplified and reformatted for publication). Here, the V-22 is almost fully converted to airplane mode, but there is enough azimuthal variation in lift to justify use of a multiple-trailer wake. An example of swept-tip blade modifications is included.

This job also illustrates the strategy for minimizing run time while achieving good convergence. The first case uses only one rotor harmonic and the default trim tolerance to quickly set up the free-wake geometry. The second case uses more rotor harmonics and reduces the trim tolerance for good loads predictions, but skips the uniform-inflow and prescribed-wake steps. This avoids the extra iterations that would otherwise be needed to converge the uniform-inflow and prescribed-wake models, especially with full harmonics and tight trim tolerance. Note that `OPINIT=7` is used to initialize the second case with the full solution from the first case. This procedure is not quite ideal for minimizing run time, because the trim matrix is recalculated for the second case, but there is nevertheless a significant time savings.

For the calculations given in the main body of this report, different values of `RELAXF`, `RELAXR`, and `TOLERC` were sometimes used to improve convergence or run time, depending on the flight condition and any rotor modifications. Also, an additional iteration of the free wake was often used to improve convergence, mostly for the 75- and 85-deg nacelle configurations.

The second example is an axial-flow job for 0-deg nacelle angle at 275 knots. The blade modifications are deleted here, but note that many inputs are identical for the two jobs and wake models.

The job-control statements are for use with the VMS operating system.

30-deg nacelles, 140 knots:

```
$ ! ** Loads analysis (single rotor) of V-22
$ ! ** 397 rpm
$ ! ** no airframe
$ ! ** match rotor power to measured power
$ ! ** assume zero flapping (not exact, but close enough)
$ ! **** -30 deg delta-3, const. XPH ****
$ !  !!!! 30 deg chord sweep from .8R;
$ !       fixed weight, 2* nominal, at .8 R,
$ !       0.25-chord offset from EA in chord plane !!!!
$ !
$ASSIGN [CAMRADII.V22]V22I.TAB        BLADEAIRFOIL1
$ASSIGN [CAMRADII.V22]V22iso.DAT      SHELLINPUT
$ASSIGN [CAMRADII.V22]30iwake.plot    PLOTFILE
$DEFINE/USER_MODE SYS$OUTPUT [CAMRADII.V22]30i140k.out
$RUN CAMRADII
 &NLJOB NCASES=2, OPINIT=7, PLFILE=1, &END
 !=========================================================================
 &NLDEF class='CASE',&END
 &NLVAL FLTASK=0,CODE='TRIM ONLY',              ! loads
 &END
 &NLDEF class='TRIM',&END
 &NLVAL
     MTRIM=3,                                  ! * trim to power
     VNAME='GOV     ','LNGCYC  ','LATCYC  ',
     MNAME='POWER   ','BCTRIM  ','BSTRIM  ',
     MHARMA=0,MHARMD=0,                        ! no airframe or drive train
     LEVEL=3,                                  ! free wake
     MHARMR=1,                                 ! flapping only
     TOLERT=5.0,                               ! default
     WINDIN=1, WKTS=140., RPM=397.,            ! * match to flight
     CPTRIM=0,PTRIM=2235.,                     ! 1/2 total aircraft HP
        GOV=55.0,LNGCYC=14.0,LATCYC=-2.0,
 &END
 &NLDEF class='TRIM ROTOR',name='ROTOR 1', &END
 &NLVAL
      OPMODE=1,                                ! blade modes
      MPSEN=0,                                 ! no sensors first case
      MASEN=0,
 &END
 &NLDEF class='ROTOR',type='STRUCTURE',name='ROTOR 1',&END
 &NLVAL
     XSP=.0575,YSP=.0332,ZSP=-.0573,              ! -30 deg delta-3
     XPH=.0317,YPH=.0341,ZPH= .0241,              ! const. XPH
 &END
 !=========================================================================
 ! Stall-delay model:
 &NLDEF class='ROTOR',type='AERODYNAMICS',name='ROTOR 1',&END
 &NLVAL
     NPANEL=17,
     REDGE=.08,.17,.25164,.32,.38775,.46,.53,.60092,.66,.71,
           .76,.80046,.84,.88,.91,.94,.97,1.0,
     NPROP=22,          ! at centers of panels plus extras to define cuff:
     RPROP=0.0, 0.04814, 0.080, 0.125, 0.211, 0.25164, 0.286,
           0.354, 0.424, 0.495, 0.565, 0.630, 0.685, 0.735,
           0.780, 0.820, 0.860, 0.895, 0.925, 0.955, 0.985, 1.0,
     ASWEEP=5*0.0, 17*1.91,
     CHORD= 0.000, 2.920, 3.000, 3.000, 2.980, 2.601, 2.566, 2.496,
            2.425, 2.351, 2.279, 2.212, 2.156, 2.105, 2.058, 2.017,
            1.977, 1.941, 1.910, 1.879, 1.848, 1.833,
     KSDL =   0.0000,    0.7609,    0.7567,    0.7567,    0.7581,    0.7485,
              0.6617,    0.5013,    0.3786,    0.2858,    0.2160,    0.1646,
```

```
            0.1288,    0.1009,    0.0788,    0.0613,    0.0456,    0.0330,
            0.0229,    0.0135,    0.0048,    0.0006,
    KSDD =  0.0000,    0.3975,    0.3863,    0.3863,    0.3892,    0.4287,
            0.3873,    0.2917,    0.2096,    0.1446,    0.0949,    0.0581,
            0.0326,    0.0127,    0.0000,    0.0000,    0.0000,    0.0000,
            0.0000,    0.0000,    0.0000,    0.0000,
    NSEN=8,                                                  ! aerodynamic sensors
    QUANT= 5,25,71,75,82,82,91,93,                           !   lambda,alpha
    AXIS=  3, 0, 0, 0, 1, 3, 0, 0,                           !   M2cl,Gamma
    OPSCL= 2, 1, 2, 2, 2, 2, 2, 2,                           !   Fx,Fz
    NAPLOT=1, 4, 1, 2, 1, 1, 1, 1,                           !   Pi,Po
    OPREF= 4, 4, 2, 4, 4, 4, 4, 4,                           !
&END
!==============================================================================
!
! Rotor modifications:
&NLDEF class='ROTOR',type='STRUCTURE',name='ROTOR 1',&END
&NLVAL ! 2* tip mass moved to 0.8R,
       ! 0.25 chord ahead of ref. line in chord plane:
       EPM(2)=0.80, XPM(2)=-0.01979, ZPM(2)=-0.01801, MASSPM(2)=0.3280,
&END
&NLDEF class='ROTOR',type='AERODYNAMICS',name='ROTOR 1',&END
&NLVAL ! sweep tip 30 deg from 0.8R:
         ASWEEP=5*0.0, 10*1.91, 7*31.91,
&END
&NLDEF class='ROTOR',type='STRUCTURE',name='ROTOR 1',&END
&NLVAL ! chord sweep tip 30 deg from 0.8R:
 XEA(54)=-0.0077, -0.0069, 0.0111, 0.0118, 0.0290, 0.0300, 0.0457,
         0.0461, 0.0489, 0.0490, 0.0518, 0.0520, 0.0547, 0.0549,
         0.0576, 0.0577, 0.0604, 0.0606, 0.0633,
 ZEA(54)=-0.0082, -0.0076, 0.0097, 0.0103, 0.0284, 0.0295, 0.0472,
         0.0480, 0.0514, 0.0515, 0.0549, 0.0551, 0.0585, 0.0586,
         0.0621, 0.0622, 0.0657, 0.0658, 0.0693,
 XQC(54)=-0.0004, -0.0004, 0.0184, 0.0184, 0.0365, 0.0364, 0.0529,
         0.0529, 0.0558, 0.0558, 0.0587, 0.0587, 0.0616, 0.0616,
         0.0645, 0.0645, 0.0673, 0.0673, 0.0701,
 ZQC(54)=0.0023, 0.0023, 0.0200, 0.0200, 0.0386, 0.0386, 0.0569,
         0.0569, 0.0604, 0.0604, 0.0639, 0.0639, 0.0674, 0.0674,
         0.0709, 0.0710, 0.0745, 0.0745, 0.0781,
&END
!==============================================================================
!
! Flight condition:
&NLDEF class='AIRFRAME',type='STRUCTURE',&END
&NLVAL OPAERO=0, OPTRAN=0,                    ! no aerodynamics or drive train
       ASHAFT=-60.0,
&END
!==============================================================================
!
! helicopter (multiple trailer with consolidation) wake model
&NLDEF class='ROTOR',type='WAKE',name='ROTOR 1',&END
&NLVAL
    OPSCEN=1,                                                ! forward flight wake
&END
&NLDEF class='ROTOR',type='WAKE',name='ROTOR 1',&END
&NLVAL OPSCEN=0,
    RFW=2.,RNW=.25,MFWG=2,REDWG=0.,FCONVN=3.,                ! forward flight
      OPFW=0,OPRUE=2,                                        ! single peak
    OPFWG=3,OPDISP=0,0,                                      ! wake geometry
      OPDWG=2,                                               ! inboard distortion
    CORE=.2,COREWG=.2,CORE(6)=.3,                            ! core size
    ITERWG=4,                                                ! convergence
  ! delete following for no consolidation
    OPCWG=2,2,KCWG=2*5.,RBCWG=2*.0,FECWG=2*1.,               ! consolidation
```

```
    CORE=.8,CORE(6)=.8,COREWG=.8,                          ! core
&END
&NLDEF class='ROTOR',type='AERODYNAMICS',name='ROTOR 1',&END
&NLVAL
    NTRAIL=17,                                             ! multiple trailer
    TEDGE=.17,.25164,.32,.38775,.46,.53,.60092,.66,.71,
          .76,.80046,.84,.88,.91,.94,.97,
    OPTRU=2,2,2,2,2,2,2,2,2,2,2,2,2,2,2,2,1,
    RGMAX=1.,                                              ! multiple trailer
&END
!=============================================================================
&NLDEF class='TRIM',&END
&NLVAL
    TOLERC=.2,ITERC=200,ITERF=5,RELAXF=.5,                 ! wake convergence
&END
&NLDEF action='end of shell',&END
&NLDEF action='end of core',&END

!#############################################################################
&NLDEF class='CASE',&END
&NLVAL NPRNTS=0,&END                                      ! simplify output
&NLDEF class='TRIM',&END
&NLVAL
    ITERU=0,                                  ! skip uniform inflow
    ITERP=0,                                  ! skip rigid wake
    MHARMR=10,                                ! 10 harmonics
    RELAXF=0.5,RELAXR=0.5,TOLERC=0.5,         ! convergence
    TOLERT=1.0,
&END
&NLDEF class='ROTOR',type='FLEXBEAM',name='ROTOR 1',&END
&NLVAL
    NSEN=1,QUANT=1,RLOAD=.05,
&END
&NLDEF class='TRIM ROTOR',name='ROTOR 1', &END
&NLVAL
     MASEN=1,NAPRNT=1,NAFILE=0,MATIME=24,MAHARM=1,
     MCSEN=1,NCPRNT=3,NCFILE=0,MCHARM=10,      ! control loads
     MBSEN=1,NBPRNT=3,NBFILE=0,MBHARM=10,      ! blade loads
     MWSEN=0,NWFILE=0,                         ! no wake file
&END
&NLDEF action='end of shell',&END
&NLDEF action='end of core',&END
!#############################################################################
$ SET NOVERIFY
```

0-deg nacelles, 275 knots:

```
$ ! ** Loads analysis (single rotor) of V-22
$ ! ** 333 rpm
$ ! ** no airframe
$ ! ** match rotor power to flight test
$ ! ** assume zero flapping (not exact, but close enough)
$ !
$ASSIGN [CAMRADII.V22]V22I.TAB     BLADEAIRFOIL1
$ASSIGN [CAMRADII.V22]V22iso.DAT   SHELLINPUT
$ASSIGN [CAMRADII.V22]0iwake.plot  PLOTFILE
$DEFINE/USER_MODE SYS$OUTPUT [CAMRADII.V22]0i275k.out
$RUN CAMRADII
 &NLJOB NCASES=2, OPINIT=7, PLFILE=1, &END
 !===============================================================================
 &NLDEF class='CASE',&END
 &NLVAL FLTASK=0,CODE='TRIM ONLY',
        OPDENS=1, ALTMSL=15000.,
 &END
 &NLDEF class='TRIM',&END
 &NLVAL
     MTRIM=3,                                  ! * trim to power
     VNAME='GOV     ','LNGCYC  ','LATCYC  ',
     MNAME='POWER   ','BCTRIM  ','BSTRIM  ',
     MHARMA=2*0,MHARMD=2*0,                    ! no airframe or drive train
     LEVEL=2*3,                                ! free wake
     MHARMR=2*1,                               ! flapping only
     WINDIN=1, WKTS=275., RPM=333.,            ! * match to flight
     CPTRIM=0,PTRIM=3830.,                     ! 1/2 total aircraft HP
        GOV=88.0,LNGCYC=0.0,LATCYC=0.0,
 &END
 &NLDEF class='TRIM ROTOR',name='ROTOR 1', &END
 &NLVAL
      OPMODE=1,                                ! blade modes
      MPSEN=0,                                 ! no sensors first case
      MASEN=0,
 &END
 &NLDEF class='AIRFRAME',type='STRUCTURE',&END
 &NLVAL OPAERO=0, OPTRAN=0,                  ! no aerodynamics or drive train
 &END
!===============================================================================
! Stall-delay model:
 &NLDEF class='ROTOR',type='AERODYNAMICS',name='ROTOR 1',&END
 &NLVAL
     NPANEL=17,
     REDGE=.08,.17,.25164,.32,.38775,.46,.53,.60092,.66,.71,
           .76,.80046,.84,.88,.91,.94,.97,1.0,
     NPROP=22,          ! at centers of panels plus extras to define cuff:
     RPROP=0.0, 0.04814, 0.080, 0.125, 0.211, 0.25164, 0.286,
           0.354, 0.424, 0.495, 0.565, 0.630, 0.685, 0.735,
           0.780, 0.820, 0.860, 0.895, 0.925, 0.955, 0.985, 1.0,
     ASWEEP=5*0.0, 17*1.91,
     CHORD= 0.000, 2.920, 3.000, 3.000, 2.980, 2.601, 2.566, 2.496,
            2.425, 2.351, 2.279, 2.212, 2.156, 2.105, 2.058, 2.017,
            1.977, 1.941, 1.910, 1.879, 1.848, 1.833,
     KSDL =   0.0000,    0.7609,    0.7567,    0.7567,    0.7581,    0.7485,
              0.6617,    0.5013,    0.3786,    0.2858,    0.2160,    0.1646,
              0.1288,    0.1009,    0.0788,    0.0613,    0.0456,    0.0330,
              0.0229,    0.0135,    0.0048,    0.0006,
     KSDD =   0.0000,    0.3975,    0.3863,    0.3863,    0.3892,    0.4287,
              0.3873,    0.2917,    0.2096,    0.1446,    0.0949,    0.0581,
              0.0326,    0.0127,    0.0000,    0.0000,    0.0000,    0.0000,
              0.0000,    0.0000,    0.0000,    0.0000,
```

```
    NSEN=8,                                                 ! aerodynamic sensors
    QUANT= 5,25,71,75,82,82,91,93,                          !   lambda,alpha
    AXIS=  3, 0, 0, 0, 1, 3, 0, 0,                          !   M2cl,Gamma
    OPSCL= 2, 1, 2, 2, 2, 2, 2, 2,                          !   Fx,Fz
    NAPLOT=1, 4, 1, 2, 1, 1, 1, 1,                          !   Pi,Po
    OPREF= 4, 4, 2, 4, 4, 4, 4, 4,                          !
&END
!========================================================================
! hover/propeller wake model
&NLDEF class='ROTOR',type='WAKE',name='ROTOR 1',action='init',&END
&NLVAL
    OPSCEN=2,TWIST=-22.,                                    ! hover wake
&END
&NLDEF class='ROTOR',type='WAKE',name='ROTOR 1',&END
&NLVAL OPSCEN=0,
    RNW=.25,OPFWG=3,OPDISP=0,0,                         ! wake model
    RICWG=.23,OPRTV=1,RTVTX=.97,                        ! tip vortex formation
    WKMODL=8*2,RFW=2.,MFWG=3,                           ! prop
!   RTVTX=.97,RFW=4.,MFWG=4,                            ! hover
&END
&NLDEF class='ROTOR',type='AERODYNAMICS',name='ROTOR 1',&END
&NLVAL
    RGMAX=1.,NTRAIL=1,                                      ! hover
    MSPAN=25,NAPLOT=8*2,                                    ! output
&END
&NLDEF class='TRIM',&END
&NLVAL
    TOLERC=.5,ITERC=100,ITERF=1,RELAXF=.5,                  ! wake convergence
&END
&NLDEF action='end of shell',&END
&NLDEF action='end of core',&END
!#########################################################################
&NLDEF class='CASE',&END
&NLVAL NPRNTS=0,&END                                    ! simplify output
&NLDEF class='TRIM',&END
&NLVAL
    ITERU=0,                                        ! skip uniform inflow
    ITERP=0,                                        ! skip rigid wake
    MHARMR=10,                                      ! 10 harmonics
    TOLERT=1.0,
&END
&NLDEF class='ROTOR',type='FLEXBEAM',name='ROTOR 1',&END
&NLVAL
    NSEN=1,QUANT=1,RLOAD=.05,
&END
&NLDEF class='TRIM ROTOR',name='ROTOR 1', &END
&NLVAL
     MASEN=1,NAPRNT=1,NAFILE=0,MATIME=24,MAHARM=1,
     MCSEN=1,NCPRNT=3,NCFILE=0,MCHARM=10,       ! control loads
     MBSEN=1,NBPRNT=3,NBFILE=0,MBHARM=10,       ! blade loads
     MWSEN=1,NWFILE=1,                          ! wake file
&END
&NLDEF action='end of shell',&END
&NLDEF action='end of core',&END
!#########################################################################
$ SET NOVERIFY
```

REFERENCES

1. Kvaternik, R. G.; Piatak, D. J., Nixon; M. W., Langston, C. W.; Singleton, J. D.; Bennett, R. L; and Brown, R. K.: An Experimental Evaluation of Generalized Predictive Control for Tiltrotor Aeroelastic Stability Augmentation in Airplane Mode of Flight. J. American Helicopter Soc., vol. 47, no. 3, July 2002.

2. Barkai, S. M.; and Rand, O.: The Influence of Composite Induced Couplings on Tiltrotor Whirl Flutter Stability. J. American Helicopter Soc., vol. 43, no. 2, April 1998.

3. Corso, L. M.; Popelka, D. A.; and Nixon, M. W.: Design, Analysis, and Test of a Composite Tailored Tiltrotor Wing. J. American Helicopter Soc., vol. 45, no. 3, July 2000.

4. Nixon, M. W.; Piatak, D. J.; Corso, L. M.; and Popelka, D. A.: Aeroelastic Tailoring for Stability Augmentation and Performance Enhancements of Tiltrotor Aircraft. J. American Helicopter Soc., vol. 45, no. 4, Oct. 2000.

5. Acree, C. W.; Peyran, R. J.; and Johnson, W.: Rotor Design Options for Improving XV-15 Whirl-Flutter Stability Margins. NASA/TP-2004-212262 and AFDD/TR-04-001, March 2004.

6. Acree, C. W.: Effects of Rotor Design Variations on Tiltrotor Whirl-Mode Stability. Tiltrotor/Runway Independent Aircraft Technology and Applications Specialists' Meeting, Arlington, Tex., Mar. 2001.

7. Acree, C. W.: Rotor Design Options for Improving V-22 Whirl-Mode Stability. American Helicopter Soc. 58th Annual Forum Proceedings, Montréal, Quebec, Canada, June 11–13, 2002.

8. Johnson, W.: CAMRAD II Comprehensive Analytical Model of Rotorcraft Aerodynamics and Dynamics. Johnson Aeronautics, Palo Alto, California, 2002.

9. Johnson, W.: Influence of Wake Models on Calculated Tiltrotor Aerodynamics. American Helicopter Soc. Aerodynamics, Acoustics, and Test and Evaluation Technical Specialists' Meeting, San Francisco, Calif., January 23–25, 2002.

10. Acree, C. W.: Effects of Blade Sweep on V-22 Whirl Flutter and Loads. American Helicopter Soc. 4th Decennial Specialist's Conference on Aeromechanics, San Francisco, Calif., Jan. 21–23, 2004.

11. Acree, C. W.: A CAMRAD II Model of the V-22 Rotor for Whirl-Flutter Analysis. NASA TM-2004-212801, July 2004.

12. Parham, T.; and Froebel, A.: V-22 EMD Intermediate Flutter and Divergence Report. Bell-Boeing Report no. 901-910-039, Bell Helicopter Textron, Sept. 1997.

13. Jenks, M. D.; and Narramore, J. C.: Final Report for the 2-D Test of Model 901 Rotor and Wing Airfoils (BSWT 592). Bell-Boeing Report No. D901-99065-1, Bell Helicopter Textron, May 1984.

14. Brunken, J. E.; and Vlaminck, R. R.: V-22 MSC/NASTRAN Airframe Vibration Analysis and Correlation. National Technical Specialists' Meeting on Rotorcraft Dynamics, Arlington, Tex., Nov. 1989.

15. Parham, T.: V-22 EMD Nonrotating Rotor Ground Vibration Test Report. Bell-Boeing Report No. 901-910-052, Bell Helicopter Textron, April 1996.

16. Popelka, D.; Sheffler, M.; and Bilger, J.: Correlation of Test and Analysis for the 1/5-Scale V-22 Aeroelastic Model. J. American Helicopter Soc., vol. 32, no. 2, April 1987.

17. Gaffey, T. M.: The Effect of Positive Pitch-Flap Coupling (Negative δ_3) on Rotor Blade Motion Stability and Flapping. J. American Helicopter Soc., vol. 14, no. 2, April 1969.

18. Srinivas, V.; Chopra, I.; and Nixon, M. W.: Aeroelastic Analysis of Advanced Geometry Tiltrotor Aircraft. J. American Helicopter Soc., vol. 43, no. 3, July 1998.

19. Mayer, R. J.: V-22 Aerodynamics Performance Demonstration: Flight Test Data Report. Bell-Boeing Report No. 901-993-486, Bell Helicopter Textron, 2000.

20. Liu, J.; and McVeigh, M. A.: Design of Swept Blade Rotors for High-Speed Tiltrotor Application. AIAA 91-3147, AIAA, AHS, and ASEE, Aircraft Design Systems and Operations Meeting, Baltimore, Md., Sept. 1991.

21. Mayda, E. A.; and van Dam, C. P.: Automated Generation of Airfoil Performance Tables Using a Two-Dimensional Navier-Stokes Solver. American Helicopter Soc. 4th Decennial Specialist's Conference on Aeromechanics, San Francisco, Calif., Jan. 2004.

22. Du, Z.; and Selig, M.S.: A 3-D Stall-Delay Model for Horizontal Axis Wind Turbine Performance Prediction. AIAA Paper 98-0021, Jan. 1998.

REPORT DOCUMENTATION PAGE

Form Approved
OMB No. 0704-0188

1. REPORT DATE *(DD-MM-YYYY)*	2. REPORT TYPE	3. DATES COVERED *(From - To)*
05-01-2005	Technical Memorandum	

4. TITLE AND SUBTITLE
Effects of Swept Tips on V-22 Whirl Flutter and Loads

5a. CONTRACT NUMBER

5b. GRANT NUMBER

5c. PROGRAM ELEMENT NUMBER

6. AUTHOR(S)
C. W. Acree, Jr.

5d. PROJECT NUMBER

5e. TASK NUMBER

5f. WORK UNIT NUMBER
21-745

7. PERFORMING ORGANIZATION NAME(S) AND ADDRESS(ES)
Ames Research Center
Moffett Field, CA 94035-1000

8. PERFORMING ORGANIZATION REPORT NUMBER
A-0513650

9. SPONSORING/MONITORING AGENCY NAME(S) AND ADDRESS(ES)
National Aeronautics and Space Administration
Washington, D.C. 20546-0001

10. SPONSORING/MONITOR'S ACRONYM(S)
NASA

11. SPONSORING/MONITORING REPORT NUMBER
NASA/TM-2005-213458

12. DISTRIBUTION/AVAILABILITY STATEMENT
Unclassified — Unlimited
Subject Category — 01
Availability: NASA CASI (301) 621-0390

13. SUPPLEMENTARY NOTES
Point of Contact: C. W. Acree, Jr., Ames Research Center, Moffett Field, CA 94035
(650) 604-5423

14. ABSTRACT

A CAMRAD II model of the V-22 Osprey tiltrotor was constructed for the purpose of analyzing the effects of blade design changes on whirl flutter. The model incorporated a dual load-path grip/yoke assembly, a swashplate coupled to the transmission case, and a drive train. A multiple-trailer free wake was used for loads calculations. The effects of rotor design changes on whirl-mode stability were calculated for swept blades and offset tip masses. A rotor with swept tips and inboard tuning masses was examined in detail to reveal the mechanisms by which these design changes affect stability and loads. Certain combinations of design features greatly increased whirl-mode stability, with (at worst) moderate increases to loads.

15. SUBJECT TERMS
V-22, Tiltrotor, Whirl flutter, Aeroelastic stability

16. SECURITY CLASSIFICATION OF:			17. LIMITATION OF ABSTRACT	18. NUMBER OF PAGES	19a. NAME OF RESPONSIBLE PERSON
a. REPORT	b. ABSTRACT	c. THIS PAGE			C. W. Acree, Jr.
Unclassified	Unclassified	Unclassified	Unclassified	46	19b. TELEPHONE *(Include area code)* (650) 604-5423